https://doi.org/10.5194/bg-2020-274
Preprint. Discussion started: 3 August 2020
© Author(s) 2020. CC BY 4.0 License.

Biogeosciences Discussions
Open Access
EGU

Reviews and syntheses: The biogeochemical cycle of silicon in the modern ocean

Paul J. Tréguer[1,2*], Jill N. Sutton[1], Mark Brzezinski[3], Matthew A. Charette[4], Timothy Devries[5], Stephanie Dutkiewicz[6], Claudia Ehlert[7], Jon Hawkings[8,9], Aude Leynaert[1], Su Mei Liu[10,11], Natalia Llopis Monferrer[1], María López-Acosta[12,13], Manuel Maldonado[13], Shaily Rahman[14], Lihua Ran[15], Olivier Rouxel[16]

[1]Univ Brest, CNRS, IRD, Ifremer, Institut Universitaire Européen de la Mer, LEMAR, Rue Dumont d'Urville, 29280, Plouzané, France

[2]State Key Laboratory of Satellite Ocean Dynamics (SOED), Ministry of Natural Resource, Hangzhou 310012, China

[3]Marine Science Institute, University of California, Santa Barbara, CA, USA

[4]Department of Marine Chemistry and Geochemistry, Woods Hole Oceanographic Institution, Woods Hole, MA 02543 USA

[5]Department of Geography, University of California, Santa Barbara, California, USA

[6]Department of Earth, Atmospheric and Planetary Sciences (DEAPS), Massachusetts Institute of Technology (MIT), Cambridge, MA 02139, USA

[7]Research Group for Marine Isotope Geochemistry, Institute for Chemistry and Biology of the Marine Environment (ICBM), Carl-von Ossietzky University Oldenburg, Germany

[8]National High Magnetic Field Lab and Earth, Ocean and Atmospheric Sciences, Florida State University, USA

[9]Interface Geochemistry, German Research Centre for Geosciences GFZ, Postdam, Germany

[10]Frontiers Science Center for Deep Ocean Multispheres and Earth System, and Laboratory of Marine Chemistry Theory and Technology MOEy, Ocean University of China, Qingdao 266100, China

[11]Laboratory for Marine Ecology and Environmental Science, Qingdao National Laboratory for Marine Science and Technology, Qingdao 266237, China

https://doi.org/10.5194/bg-2020-274
Preprint. Discussion started: 3 August 2020
© Author(s) 2020. CC BY 4.0 License.

Biogeosciences Discussions Open Access EGU

[12]Institute of Marine Research (IIM-CSIC), Rúa de Eduardo Cabello 6, Vigo 36208, Pontevedra, Spain

[13]Department of Marine Ecology. Center for Advanced Studies of Blanes (CEAB-CSIC), Acceso Cala St. Francesc 14, Blanes 17300, Girona, Spain

[14]Department of Marine Science, University of Southern Mississippi, Stennis Space Center, MS 39529, USA

[15]Second Institute of Oceanography, Ministry of Natural Resources, P. R. China

[16] IFREMER, Centre de Brest, Technopôle Brest Iroise, Plouzané, France

Correspondance: Paul Tréguer (paul.treguer@univ-brest.fr) and Jill Sutton (jill.sutton@univ-brest.fr)

https://doi.org/10.5194/bg-2020-274
Preprint. Discussion started: 3 August 2020
© Author(s) 2020. CC BY 4.0 License.

Biogeosciences Discussions

Abstract

The element silicon (Si) is required for the growth of silicified organisms in marine environments, such as diatoms, which consume vast amounts of Si together with N, P, and C, connecting the biogeochemical cycles of these elements. Thus, understanding the Si cycle in the ocean is critical for understanding issues such as carbon sequestration by the ocean's biological pump. In this review, we show that recent advances in process studies indicate that total Si inputs and outputs, to and from the world ocean, are 57 % and 18 % higher, respectively, than previous estimates. We also update the total ocean silicic acid inventory value, which is about 24 % higher than previously estimated. These changes are significant, modifying factors such as the geochemical residence time of Si, which is now about 8,000 years and two times faster than previously assumed. In addition, we present an updated value of the global annual pelagic biogenic silica production (255 Tmol-Si yr^{-1}) based on new data from 49 field studies and 18 model outputs, and provide a first estimate of the global annual benthic biogenic silica production due to sponges (6 Tmol-Si yr^{-1}). Given these important modifications, we address the steady state hypothesis of the Si cycle for past and modern oceans, and propose a possible steady state scenario for the global ocean (inputs = outputs = 14.8 Tmol-Si yr^{-1}) and boundary exchange zone. Case studies for future programs are highlighted, and potential impacts of global change on the marine Si cycle discussed.

1. Introduction

Silicon, the seventh-most abundant element in the universe, is the second-most abundant element of the Earth's crust. The weathering of the Earth's crust by CO_2-rich rain water, a key process in the control of atmospheric CO_2, results in the generation of silicic acid (dSi; $Si(OH)_4$) in aqueous environments. Silicifiers use dSi to precipitate biogenic silica (bSi; SiO_2) as internal (Moriceau et al., 2019) and/or external (Maldonado et al., 2019) structures. They are among the most important aquatic organisms, including micro-organisms (e.g. diatoms, rhizarians, silicoflagellates, several species of choanoflagellates), and macro-organisms (e.g. siliceous sponges). Phototrophic silicifiers, such as diatoms, globally consume vast amounts of Si concomitantly with nitrogen, phosphorous and inorganic carbon, connecting the biogeochemistry of these elements and contributing to the sequestration of atmospheric CO_2 in the ocean (Tréguer & Pondaven, 2000). Heterotrophic organisms like rhizarians, choanoflagellates and sponges produce bSi independent of the photoautrophic processing of C and N, a bSi that has been named "dark silica" (Maldonado et al., 2012, 2019).

https://doi.org/10.5194/bg-2020-274
Preprint. Discussion started: 3 August 2020
© Author(s) 2020. CC BY 4.0 License.

Understanding the Si cycle is critical for understanding the functioning of marine food webs, biogeochemical cycles, and the biological carbon pump. Herein, we review recent advances in field observations and modelling that have changed our understanding of the global Si cycle and provide an update of four of the six net annual input fluxes and of all the output fluxes previously estimated by Tréguer & De La Rocha (2013). Taking into account numerous field studies in different marine provinces and model outputs, we re-estimate the "canonical" value of Si production (Nelson et al., 1995), review the potential contribution of rhizarians (Llopis Monferrer et al., 2020) and picocyanobacteria (Ohnemus et al., 2016), and give an estimate of the total bSi production by siliceous sponges using recently published data on sponge bSi in marine sediments (Maldonado et al., 2019). We discuss the question of the balance/imbalance of the marine Si biogeochemical cycle at different time scales, and propose a possible steady state scenario for the modern ocean, with inputs balancing outputs at 14.8 Tmol yr^{-1} (Fig. 1). Finally, we address the question of the potential impact of anthropogenic activities on the global Si cycle and suggest guidelines for future research endeavours.

2. Advances in input fluxes

As illustrated in Figure 1, silicic acid (dSi) is delivered to the ocean through six pathways, which all ultimately derive from the weathering of the Earth's crust (Tréguer & De La Rocha, 2013). All fluxes are given with standard deviations.

2.1 Riverine (F_R) and Aeolian (F_A) contributions

The best estimate for the riverine input (F_R) of dSi, based on data representing 60 % of the world river discharge and a discharge-weighted average dSi riverine concentration of 158 µM-Si (Dürr et al., 2011), remains at F_{RdSi} = 6.2 (± 1.8) Tmol-Si yr^{-1} (Tréguer & De La Rocha, 2013). However, Si is transferred from the terrestrial to the riverine system, not only as dSi but also as particulate Si, in either its crystallised or amorphous form (Dürr et al., 2011). According to Saccone et al. (2007), the term "amorphous silica" (aSi) gathers biogenic silica (bSi, from phytoliths, freshwater diatoms, sponge spicules), altered bSi, and pedogenic silicates, the three of which can have similar high solubilities and reactivities to aSi. Delivery of aSi to the fluvial system has been reviewed by Frings et al. (2016) and they suggested a value of F_{RaSi} = 1.9 (± 1.0) Tmol-Si yr^{-1}. Therefore, total F_R = 8.1 (± 2.0) Tmol-Si yr^{-1}.

Regarding the aeolian dust deposition into the ocean (Tegen & Kohfeld, 2006) and subsequent release of dSi via dust dissolution in seawater, no progress has been made since Tréguer and De La Rocha (2013), which summed the flux of particulate dissolvable silica and wet deposition of dSi through precipitations. Thus, our best estimate for F_A remains 0.5 (± 0.5) Tmol-Si yr^{-1}.

https://doi.org/10.5194/bg-2020-274
Preprint. Discussion started: 3 August 2020
© Author(s) 2020. CC BY 4.0 License.

2.2 Dissolution of minerals (F_W)

In agreement with Tréguer et al. (1995), Tréguer and De La Rocha (2013) considered benthic Si fluxes from non-siliceous sediments between ~10-20 mmol m^{-2} yr^{-1}, which gave an estimate of F_w = 1.9 (± 0.7) Tmol-Si yr^{-1} if extrapolated to 120 Mkm^2 zone of opal-poor sediments in the global ocean.

About 15-20 Gt yr^{-1} river-derived lithogenic particles are deposited along the margins and shelves (e.g. Syvitskia et al., 2003, also see Fig. 2). Dissolution experiments with river sediments or basaltic glass in seawater showed that 0.08-0.17% of the Si in the solid phase was released within a few days to months (e.g., Jones et al., 2012; Morin et al., 2015; Oelkers et al., 2011; Pearce et al., 2013). However, the high solid-to-solution ratios in these experiments increased the dSi concentration quickly to near-equilibrium conditions inhibiting further dissolution, which prevents direct comparison with natural sediments. Field observations and subsequent modelling of Si release range around 0.5 – 5 % yr^{-1} (e.g., Arsouze et al., 2009; Jeandel and Oelkers, 2015). On the global scale, Jeandel et al. (2011) estimated the total flux of dissolution of minerals to range between 0.7 - 5.4 Tmol-Si yr^{-1}, i.e. similar to the dSi river flux, but this estimate is based on the assumption of 1 - 3 % congruent dissolution of sediments for a large range of lithological composition which, so far, is not proven. A recent study by Frings (2017) estimates that "non-biogenic silica" sediments (i.e. clays and calcareous sediments, which cover about 78% of the ocean area) may contribute up to 44.9 Tmol-Si yr^{-1} via benthic diffusive Si flux. However, according to lithological descriptions given in GSA Data Repository 2015271 some of the "non-biogenic silica" sediment classes described in this study may contain significant bSi, which might explain Frings' high estimate for F_W.

Therefore, our best estimate for this component remains 1.9 (± 0.7) Tmol-Si yr^{-1}.

2.3 Submarine groundwater (F_{GW})

Since 2013, several papers have sought to quantify the global oceanic input of dissolved Si (dSi) from submarine groundwater discharge (SGD), which includes terrestrial (freshwater) and marine (saltwater) components (Fig. 2). Silicic acid inputs through SGD may be considerable, in places similar to or in excess of riverine input. For instance, in the Bay of Bengal, Georg et al. (2009) estimated this input to be 0.093 Tmol-Si yr^{-1}, which is ~ 66% of the Ganges-Brahmaputra river flux of dSi to the ocean. At world scale, Tréguer and De La Rocha (2013)'s best estimate for F_{GW} was 0.6 (± 0.6) Tmol-Si yr^{-1}. More recently, Rahman et al. (2019) used a global terrestrial SGD flux model weighted according to aquifer lithology (Beck et al., 2013) in combination with a compilation of dSi in shallow water coastal aquifers to derive a terrestrial groundwater input of dSi to the world ocean of 0.7 (± 0.1) Tmol-Si yr^{-1}. This new estimate,

https://doi.org/10.5194/bg-2020-274
Preprint. Discussion started: 3 August 2020
© Author(s) 2020. CC BY 4.0 License.

with its relatively low uncertainty, represents the lower limit flux of dSi to the ocean via SGD. The marine component of SGD, driven by a range of physical processes such as density gradients or waves and tides, is fed by seawater that circulates through coastal aquifers or beaches via advective flow paths (Fig. 2; also see Fig. 1 of Li et al., 1999). This circulating seawater may become enriched in dSi through bSi or mineral dissolution, the degree of enrichment being determined by subsurface residence time and mineral type (Anschutz et al., 2009; Ehlert et al. 2016a; Techer et al., 2001).

Several lines of evidence show that the mineral dissolution (strictly corresponding to net dSi input) may be substantial (e.g., Ehlert et al., 2016b). Focusing on processes occurring in tidal sands, Anschultz et al. (2009) showed that they can be a biogeochemical reactor for the Si cycle. Extrapolating laboratory-based dissolution experiments performed with pure quartz, Fabre et al. (2019) calculated that the potential flux of dissolution of quartz of sandy beaches, driven by wave and tidal action, at world scale (Luijendijk et al., 2018) could be 3.2 (± 1.0) Tmol Si yr^{-1}. However, this estimate, not validated by field experiments, is not well constrained (Supplement, section 1). Cho et al. (2018), using a ^{228}Ra inverse model and groundwater dSi/^{228}Ra ratios, estimate the total (terrestrial + marine) SGD dSi flux to the ocean to be 3.8 (± 1.0) Tmol-Si yr^{-1}; this represents a realistic upper limit value for SGD's contribution to the global ocean dSi cycle. For the time being, without systematic data that corroborates the net input of dSi through the circulation of the marine component of SGD (e.g., porewater $\delta^{30}Si$, paired dSi and ^{228}Ra measurements), we estimate the range of net input of dSi through total SGD as 0.7 Tmol-Si yr^{-1} (Rahman et al., 2019) to 3.8 Tmol-Si yr^{-1} (Cho et al., 2018), with an average, i.e. F_{GW} = 2.3 (±1.1) Tmol-Si yr^{-1}, which is about three times larger than Tréguer & De La Rocha (2013).

2.4 (Sub)polar glaciers (F_{ISMW})

This flux was not considered by Tréguer & De La Rocha (2013). Since 2013, Tréguer (2014) and Hawkings et al. (2017) have identified polar glaciers as sources of Si to marine environments. The current best estimate of discharge weighted dSi concentration in (sub)Arctic glacial meltwater rivers lies between 20-30 µM although concentrations ranging between 3 and 425 µM have been reported (Meire et al., 2016; Hatton et al., 2019). Only one value currently exists (Michaud et al., 2016) for dSi from subglacial meltwater in Antarctica (126 µM) and iceberg dSi concentrations are poorly quantified (~ 5 µM) (Meire et al., 2016). Glacier meltwater typically contains high suspended sediment concentrations due to intense physical erosion with a relatively high dissolvable aSi component (0.3-1.5% dry weight) equating to concentrations of 70-340 µM (Hawkings, 2018; Hatton et al., 2019). Iceberg aSi concentrations are lower (28-83 µM) (Hawkings et al., 2017). This particulate phase appears fairly soluble in

https://doi.org/10.5194/bg-2020-274
Preprint. Discussion started: 3 August 2020
© Author(s) 2020. CC BY 4.0 License.

seawater (Hawkings et al., 2017), and large benthic dSi fluxes in glacially influenced shelf seas have been observed (Hendry et al., 2019; Ng et al., 2020). Silicic acid input from (sub)polar glaciers is estimated to be 0.04 (± 0.04) Tmol-Si yr^{-1}. If the aSi flux is considered then this may provide an additional 0.29 (± 0.22) Tmol-Si yr^{-1}, with a total F_{ISMW} (= dSi+aSi) input estimate of 0.33 (± 0.26) Tmol-Si yr^{-1}.

2.5 Hydrothermal activity (F_H)

Tréguer & De La Rocha (2013)'s estimate for F_H was 0.6 (± 0.4) Tmol-Si yr^{-1}. Seafloor hydrothermal activity at mid-ocean ridges (MOR) and ridge-flanks is one of the fundamental processes controlling the exchange of heat and chemical species between seawater and ocean crust (Wheat & Mottl, 2000). A major challenge limiting our current models of both heat and mass flux (e.g. Si flux) through the seafloor is estimating the distribution of the various forms of hydrothermal fluxes, including focused vs. diffuse and ridge axis vs. ridge flank fluxes. Estimates of the Si flux for each input are detailed below.

Axial and near axial hydrothermal fluxes settings: The best estimate of the heat flux at ridge axis (i.e. crust 0–0.1 Ma in age) is 1.8 (± 0.4) TW, while the heat flux in the near-axial region (i.e. crust 0.1–1 Ma in age) has been inferred at 1.0 (± 0.5) TW (Mottl, 2003). The conversion of heat flux to hydrothermal water and chemical fluxes requires assumptions regarding the temperature at which this heat is removed. For an exit temperature of 350 (± 30)°C typical of black smoker vent fluids, and an associated enthalpy of 1,500 (± 190) J g^{-1} at 450–1000 bars and heat flux of 2.8 (± 0.4) TW, a maximum seawater flux of 5.9 (± 0.8) 10^{16} g yr^{-1} is required (Mottl, 2003). High temperature hydrothermal dSi flux is calculated using a dSi concentration of 19 (± 11) mmol kg^{-1}, which is the average concentration in hydrothermal vent fluids that have an exit temperature > 300°C. This estimate is based on a compilation of > 100 discrete vent fluid data, corrected for seawater mixing (i.e. end-member values at Mg=0, Edmond et al., 1979) and phase separation. Although the chlorinity of hot springs varies widely, nearly all of the reacted fluid, whether vapor or brine, must eventually exit the crust within the axial region. The integrated hot spring flux must therefore have a chlorinity similar to that of seawater. The relatively large range of dSi concentrations in high-temperature hydrothermal fluids likely reflect the range of geological settings (e.g. fast- and slow-spreading ridges) and host-rock composition (ultramafic, basaltic or felsic rocks). Because dSi enrichment in hydrothermal fluids result from mineral-fluid interactions at depth, and is mainly controlled by solubility of secondary minerals and quartz (Mottl 1983; Von Damm et al. 1991), it is also possible to obtain a theoretical estimate of the concentration of dSi in global hydrothermal vent fluids. Under the

https://doi.org/10.5194/bg-2020-274
Preprint. Discussion started: 3 August 2020
© Author(s) 2020. CC BY 4.0 License.

conditions of temperature and pressure (i.e. depth) corresponding to the base of the upflow zone of high temperature (>350 - 450°C) hydrothermal systems, dSi concentrations between 16 to 22 mmol kg^{-1} are calculated, which is in good agreement with measured values in end-member hydrothermal fluids. Using a dSi concentration of 19 (± 3.5) mmol kg^{-1} and water flux of 4.8 (± 0.8) $x10^{16}$ g yr^{-1}, we determine an axial hydrothermal Si flux of 0.91 (± 0.29) Tmol-Si yr^{-1}. It should be noted, however, that high-temperature hydrothermal fluids may not be entirely responsible for the transport of all the axial hydrothermal heat flux (Elderfield and Schultz, 1996; Nielsen et al., 2006). Because dSi concentrations in diffuse hydrothermal fluids is not significantly affected by subsurface Si precipitation during cooling of the hydrothermal fluid (Escoube et al., 2015), we however consider that the global hydrothermal Si flux is not strongly affected by the nature (focused vs. diffuse) of axial fluid flow.

Ridge flank hydrothermal fluxes: Chemical fluxes related to seawater-crust exchange at ridge flanks has been previously determined through direct monitoring of fluids from low-temperature hydrothermal circulation (Wheat and Mottl, 2000). Using basaltic formation fluids from the 3.5 Ma crust on the eastern flank of the Juan de Fuca Ridge (Wheat and McManus, 2005), determined a global flux of 0.011 Tmol-Si yr^{-1} for warm ridge flank. This estimate is based on the measured Si anomaly associated with warm spring (0.17 mmol kg^{-1}) and a ridge flank fluid flux determined using oceanic Mg mass balance, therefore assuming that the ocean is at steady-state with respect to Mg. More recent results of basement fluid compositions in cold and oxygenated ridge flank settings (e. g. North Pond, Mid-Atlantic Ridge) also confirms that incipient alteration of volcanic rocks may result in significant release of Si to circulating seawater (Meyer et al., 2016). The total heat flux through ridge flanks, from 1 Ma crust to a sealing age of 65 Ma, has been estimated at 7.1 (± 2) TW. Considering that most of ridge-flank hydrothermal power output should occur at cool sites (< 20°C), the flux of slightly altered seawater could range from 0.2 to 2 $x10^{19}$ g yr^{-1}, rivaling with the flux of river water to the ocean of 3.8 $x10^{19}$ g yr^{-1} (Mottl, 203). Using this estimate and Si anomaly of 0.07 mmol-Si kg^{-1} reported in cold ridge flank setting from North Pond (S18), a Si flux of 0.14 to 1.4 Tmol-Si yr^{-1} for cold ridge flank could be determined. Because of the large volume of seawater interacting with oceanic basalts in ridge flank settings, even a small chemical anomaly resulting from reactions within these cold systems could result in a globally significant elemental flux. Hence, additional studies are required to better determine the importance of ridge flanks to oceanic Si budget.

https://doi.org/10.5194/bg-2020-274
Preprint. Discussion started: 3 August 2020
© Author(s) 2020. CC BY 4.0 License.

Combining axial and ridge flank estimates, the best estimate for F_H is now 1.7 (± 0.8) Tmol-Si yr^{-1}, about three times larger than Tréguer & De La Rocha (2013)'s estimate.

2.6 Total net inputs (Table 1A)

Total Si input = 8.1(± 2.0) ($F_{R(dSi+aSi)}$) + 0.5 (± 0.5) (F_A) + 1.9 (± 0.7) (F_W) + 2.3 (± 1.1) (F_{GW}) + 0.3 (± 0.3) (F_{ISMW}) + 1.7 (± 0.8) (F_H) = **14.8 (± 2.6) Tmol-Si yr^{-1}**.

The uncertainty of the total Si inputs (and total Si outputs, section 3) has been calculated using the error propagation method (Bevington and Robinson, 2003). This has been done for the total fluxes and the individual flux estimates.

3. Advances in output fluxes

3.1 Long-term burial of planktonic biogenic silica in sediments (F_B)

Long-term burial of bSi, which generally occurs below the top 10-20 cm of sediment, was estimated by Tréguer & De La Rocha (2013) to be 6.3 (± 3.6) Tmol-Si yr^{-1}. The burial rates are highest in the Southern Ocean (SO), the North Pacific Ocean, the equatorial Pacific Ocean, and in the coastal and continental margin zone CCMZ (DeMaster et al., 2002; Hou et al., 2019; Rahman et al., 2017).

Since DeMaster (2002) the burial rate in the open ocean remains unchanged at >1.04 (± 0.34) Tmol-Si yr^{-1}. Pichevin et al. (2014) have shown that bSi burial may also be enhanced in Fe limited regions in the open ocean, which include the SO, warranting further study on the physical and chemical factors that control the form of burial output fluxes of Si. For the SO, particularly in the "opal belt" zone (Geibert et al., 2005), to correct for processes like winnowing and focusing (leading to under- and over-estimation of uncorrected sedimentation and burial rates), the burial rates are typically normalized using the particle reactive nuclide ^{230}Th (Geibert et al., 2005). Chase et al. (2015) has revised upward Tréguer & De La Rocha (2013)'s estimate. According to these authors the best estimate for the SO burial rate, south of 40°S, is now 2.3 (± 1.0) Tmol-Si yr^{-1}.

Regarding the CCMZ, estimates of silica burial rates have been usually determined from carbon burial rates using a Si : C ratio of 0.6 (DeMaster 2002). However, we now have independent estimates of marine organic C and of total initial bSi burial (e.g. Aller et al., 1996; Aller et al., 2008; Galy et al., 2007; Rahman et al., 2016, 2017). It has been shown that the initial bSi burial in sediment evolved as unaltered bSi or as authigenically formed alumino-silicate phase (Rahman et al., 2017). The Si : C burial ratios of residual marine plankton post-remineralization in tropical and subtropical deltaic systems are much greater (2.4 - 11) than the 0.6 Si:C burial

https://doi.org/10.5194/bg-2020-274
Preprint. Discussion started: 3 August 2020
© Author(s) 2020. CC BY 4.0 License.

ratio assumed for continental margin deposits (DeMaster, 2002). Therefore, the sedimentary Si:C preservation ratios are suggested to depend on differential remineralization pathways of marine bSi and C_{org} under different diagenetic regimes (Aller et al., 1996). Partitioning of ^{32}Si activities between bSi and mineral pools in tropical deltaic sediments indicate rapid and near–complete transformation of initially deposited bSi to authigenic clay phases (Rahman et al., 2017). For example, in subtropical/temperate deltaic and estuarine deposits, ^{32}Si activities signal approximately ~50% of initial bSi_{opal} delivery to sediments (Rahman et al., 2017). Using the ^{32}Si technique Rahman et al. (2019) provided an updated estimate of bSi burial for the CCMZ of 3.7 (± 2.1) Tmol-Si yr^{-1}, higher than Tréguer and De La Rocha (2013)'s estimate of 3.3 (± 2.1) Tmol-Si yr^{-1} based on the Si:C method of DeMaster (2002).

Combining DeMaster (2002)'s burial rate of the open ocean zone with these new estimates for the SO and the CCMZ gives a revised global total burial flux, F_b, of > 7.0 (± 2.4) Tmol-Si yr^{-1}, 11 % larger than Tréguer and De La Rocha (2013)'s estimate.

3.2 Deposition and long-term burial of sponge silica (F_{SP})

Tréguer and De La Rocha (2013)'s estimate for F_{SP}, the net sink of sponge bSi in sediments of continental margins, was 3.6 (± 3.7) Tmol Si yr^{-1}. The longevity of sponges, ranging from years to millennia, temporally decouples the process of skeleton production from the process of deposition to the sediments (Jochum et al., 2017). While sponges slowly accumulate bSi over their long and variable lifetimes (depending on the species), the deposition to the sediments of the accumulated bSi is a relatively rapid process after sponge death, lasting days to months (Supplement, section 2). Tréguer and De La Rocha (2013)'s estimate was calculated as the difference between the sponge dSi demand on continental shelves (3.7 (± 3.6) Tmol Si yr^{-1}) — estimated from silicon consumption rates available for few sublittoral sponge species (Maldonado et al., 2011) —, and the flux of dSi from the dissolution of sponge skeletons in continental shelves (0.15 (± 0.15) Tmol Si yr^{-1}). This flux was tentatively estimated from the rate of dSi dissolution from a rare, unique glass sponge reef at Bristish Columbia (Canada) (Chu et al., 2011) and which is unlikely to be representative of the portion of sponge bSi that dissolves back as dSi after sponge death and before their burial in the sediments. To improve the estimate, Maldonado et al. (2019) used microscopy to access the amount of sponge silica that was actually being buried in the marine sediments using 17 sediment cores representing different marine environments. The deposition of sponge bSi was found to be one order of magnitude more intense in sediments of continental margins and seamounts than on continental rises and central basin bottoms. By assuming that the rate of sponge silica deposition in each core had been approximately constant through the Holocene, the new best estimate (Maldonado et al. (2019)

https://doi.org/10.5194/bg-2020-274
Preprint. Discussion started: 3 August 2020
© Author(s) 2020. CC BY 4.0 License.

for F_{SP} is 1.7 (± 1.6) Tmol-Si yr^{-1}, i.e. two times smaller than Tréguer and De La Rocha's preliminary estimate.

3.2 Reverse Weathering flux (F_{RW})

The previous estimate for this output flux, provided by Tréguer & De La Rocha (2013), F_{RW} = 1.5 (± 0.5) Tmol-Si yr^{-1}, was determined using indirect evidence since the influence of reverse weathering on the global Si cycle prior to 2013 was poorly understood. For example, reverse weathering reactions at the sediment–water interface were previously thought to constitute a relatively minor sink (0.03 – 0.6 Tmol-Si yr^{-1}) of silica in the ocean (DeMaster, 1981). The transformation of bSi to a neoformed aluminosilicate phase, or authigenic clay formation, was assumed to proceed slowly (> 10^4 - 10^5 years) owing principally to the difficulty of distinguishing the contribution of background lithogenic or detrital clays using the common leachates employed to quantify bSi (DeMaster, 1981). Recent direct evidence supporting the rapid formation of authigenic clays comes from tropical and subtropical deltas (Michalopoulos & Aller, 1995; Rahman et al., 2016, 2017; Zhao et al., 2017) and several geochemical tools show that authigenic clays may form ubiquitously in the global ocean (Baronas et al., 2017; Ehlert et al., 2016a; Michalopoulos & Aller, 2004). Activities of cosmogenic ^{32}Si ($t_{1/2}$ ~140 yrs), incorporated into bSi in the surface ocean, provide demonstrable proof of rapid reverse weathering reactions by tracking the fate of bSi upon delivery to marine sediments (Rahman et al., 2016). By differentiating sedimentary bSi storage between unaltered bSi (bSi_{opal}) and diagenetically altered bSi ($bSi_{altered}$) in the proximal coastal zone, ^{32}Si activities in these pools indicate that 3.7 Tmol-Si yr^{-1} is buried as unaltered bSi_{opal} (also see Supplement, section2) and 4.7 (± 2.3) Tmol-Si yr^{-1} as authigenic clays (bSi_{clay}) on a global scale. Here, we adopt 4.7 Tmol-Si yr^{-1} for F_{RW} representing about three times the Tréguer & De La Rocha (2013)'s value.

3.3 Total net output (Table 1A)

Total Si output = 7.0 (± 2.3) ($F_{B(net\ deposit)}$) + 4.7 (± 2.3) (F_{RW}) + 1.7 (± 1.6) (F_{SP}) = **13.4 (± 3.7) Tmol-Si yr^{-1}**.

4. Advances in biological fluxes

4.1 bSi annual pelagic production

4.1.1 from field data

The "canonical" value for global gross marine bSi pelagic production is 240 (± 40) Tmol-Si yr^{-1} (Nelson et al., 1995). Since 1995, the number of field studies of bSi production (using either the ^{30}Si tracer method, Nelson & Goering (1977) or the ^{32}Si method (Tréguer et al., 1991; Brzezinski & Phillips, 1997), has grown substantially from 15 (1995) to 49 in 2019, allowing

https://doi.org/10.5194/bg-2020-274
Preprint. Discussion started: 3 August 2020
© Author(s) 2020. CC BY 4.0 License.

the first estimate based on empirical silica production rate measurements (Fig. 3, and Supplement, section 3). It is usually assumed that the silica production, as measured by the above methods, is mostly supported by diatoms, with some unknown (but minor) contribution of other planktonic species.

The silica production rates measured during 49 field campaigns were assigned to Longhurst provinces (Longhurst, 2007; Longhurst et al., 1995) based on location, with the exception of the Southern Ocean, where province boundaries were defined according to Tréguer & Jacques (1992). Extrapolating these "time-and-space-limited" measurements of bSi, spatially to a biogeographic province, and annually from the bloom phenology for each province (calculated as the number of days where the chlorophyll concentration is greater than the average concentration between the maximum and the minimum values) results in annual silica production estimates for 26 of the 56 world ocean provinces. For the "ocean basin" estimate (Table 2), the annual production of all provinces in a basin were averaged, and then extrapolated by basin area. For the "domain" estimate (Table 2), the averages from provinces were subdivided among coastal, Southern Ocean, and open ocean domains, and extrapolated based on the area of each domain. Averaging the "ocean basin" and the "domain" annual estimates (Table 2), our best estimate for the global marine bSi production is 267 (± 18) Tmol-Si yr^{-1} (Table 2).

4.1.2 bSi annual pelagic production from models

Estimates of bSi production were also derived from satellite productivity models, and from global ocean biogeochemical models (GOBMs).

For the estimates based on satellite productivity models, we used global net primary production (NPP) estimates from the carbon-based productivity model (Westberry et al., 2008) and the vertically generalized productivity model (VGPM) (Behrenfeld & Falkowski, 1997). NPP estimates from these models were divided into oligotrophic (< 0.1 µg Chl a L^{-1}), mesotrophic (0.1 - 1.0 µg Chl a L^{-1}) and eutrophic (> 1.0 µg Chl a L^{-1}) areas (Carr et al., 2006). The fraction of productivity by diatoms in each area was determined using the DARWIN model (Dutkiewicz et al., 2015) resulting in diatoms accounting for 29% of the global production. Each category was further subdivided into High Nutrient Low Chorophyll (HNLC) (>5 µM surface nitrate, World Ocean Atlas 2015, Garcia et al., 2014), coastal (< 300 km from a coastline) and open ocean (remainder) regions for application of Si:C ratios to convert to diatom silica production. Si:C ratios were 0.52 for HNLC regions, 0.065 for the open ocean and 0.13 for the coastal regions, reflecting the effect of Fe limitation in HNLC areas (Franck et al. 2000), of Si limitation for uptake in the open ocean (Brzezinski et al., 1998, 2011; Brzezinski & Nelson,

https://doi.org/10.5194/bg-2020-274
Preprint. Discussion started: 3 August 2020
© Author(s) 2020. CC BY 4.0 License.

1996; Krause et al., 2012), and of replete conditions in the coastal zone (Brzezinski, 1985). Silica production estimates where then subdivided between coast (within 300 km of shore), open ocean and Southern Ocean (northern boundary 43°S from Australia to South America, 34.8°S from South America to Australia) and summed to produce regional estimates (Table 2). From satellite productivity models our best estimate for the global marine bSi production is 207 (± 23) Tmol-Si yr^{-1} (Table 2).

A second model-based estimate of silica production considered 18 numerical GOBMs models of the marine silica cycle that all estimated global silica export from the surface ocean (Aumont et al., 2015; Bernard et al., 2011; De Souza et al. 2014; Dunne et al., 2007; Dutkiewicz et al., 2015; Gnanadesikan et al., 1999; Heinze et al., 2003; Holzer et al., 2014; Jin et al., 2006; Matsumoto et al., 2013; Pasquier & Holzer, 2017; Roshan et al., 2018; Sarmiento et al., 2007; Usbeck, 1999; Ward et al., 2012; Wischmeyer et al., 2003). These models include variants of the MOM, HAMOCC OCIM, DARWIN, cGENIE and PICES models. Export production was converted to gross silica production by using a silica dissolution-to-production (D:P) ratio for the surface ocean of 0.58 for the open ocean and 0.51 for coastal regions (Tréguer & De La Rocha, 2013). Model results were first averaged within variants of the same model, and then averaged across models to eliminate biasing the average to any particular model. From GOBMs our best estimate for the global marine bSi production is 276 (± 23) Tmol-Si yr^{-1} (Table 2). Averaging the estimates calculated from satellite productivity models and GOBMs give a value of 242 (± 49) Tmol-Si yr^{-1} for the global marine bSi production (Table 2).

4.1.3 Best estimate for bSi annual pelagic production

Using a simple average of the "field" and "model" estimates, the revised best estimate of global marine gross bSi production, mostly due to diatoms, is now F_{Pgross} = **255 (± 52) Tmol-Si yr^{-1}**, not significantly different from the Nelson et al. (1995)'s canonical value.

In the Southern Ocean (SO), a key area for the world ocean Si cycle (DeMaster, 1981), there is some disagreement among the different methods of estimating bSi production. Field studies give an estimate of 67 Tmol-Si yr^{-1} for the annual gross production of silica in the SO, close to the estimate calculated using satellite productivities models (Table 2). However, the SO estimate calculated from numerical models of the global silica cycle (Dutkiewicz et al., 2015; Gnanadesikan et al. 1999; Holzer et al, 2014; Jin et al. 2006; Matsumoto et al., 2013; Roshan et al., 2018; Sarmiento et al., 2007), is about two times larger than that calculated from silica production studies (Table 2). GOBMs include a very limited number of functional groups of phytoplankton, with some only including two: small phytoplankton and diatoms. As such these

https://doi.org/10.5194/bg-2020-274
Preprint. Discussion started: 3 August 2020
© Author(s) 2020. CC BY 4.0 License.

models are likely to overestimate the role that diatoms play, especially in the SO. See also Supplement, section 4.

4.1.4 Estimates of the bSi production of other pelagic organisms

Regarding phytoplanktonic organisms other than pelagic diatoms, extrapolations from field and laboratory work show that the contribution of picocyanobacteria (like *Synechococcus*, Baines et al. 2012, Brzezinski et al., 2017; Krause et al., 2017) to the world ocean accumulation of bSi is < 20 Tmol-Si yr^{-1}.

According to Llopis Monferrer et al. (2020), the gross silica production of rhizarians, siliceous protists, in the 0-1000 m layer might range between 2 – 58 Tmol-Si yr^{-1}, about 50% of it occurring in the 0-200 m layer.

Note that these preliminary estimates of bSi accumulation or production by picocyanobacteria and rhizarians are within the uncertainty of our best estimate of F_{Pgross}.

4.2 Estimates of the bSi production of benthic organisms

Note that the above updated estimate of the pelagic production does not take into account bSi production by benthic organisms like benthic diatoms and sponges. Our knowledge of these production terms is not well developed for benthic diatoms and no robust estimate is available for bSi annual production of benthic diatoms at global scale (Supplement, section 4).

Recently, substantial progress has been made for silica deposition by siliceous sponges. Laboratory and field studies reveal that sponges are highly inefficient in the molecular transport of dSi and, consequently in the bSi production, compared to diatoms and particularly when dSi concentrations are lower than 75 µM, a situation that applies virtually to most ocean areas (Maldonado et al., 2020). On average, sponge communities are known to produce bSi at rates that are about 2 orders of magnitude smaller than those measured for diatom communities (Maldonado et al., 2012). Because sponge populations are not homogeneously distributed on the marine bottoms, and extensive, poorly mapped and unquantified aggregations of heavily silicified sponges occur in deep sea of all oceans, the global standing crop of sponges is very difficult to be constrained and the annual bSi production attained by such standing crop even more difficult to estimate. A first tentative estimate of bSi production for sponges on continental shelves, where sponge biomass can be more easily approximated, ranged widely, from 0.87 to 7.39 Tmol-Si yr^{-1}, because of persisting uncertainties in estimating sponge standing crop (Maldonado et al., 2012). A way to estimate the global annual bSi production by sponges without knowing their standing crop is to retrace bSi production values from the amount of sponge bSi that is annually being deposited to the ocean bottom, after assuming that, in the long run, the standing crop of sponges in the ocean is in equilibrium (i.e, it is neither progressively

https://doi.org/10.5194/bg-2020-274
Preprint. Discussion started: 3 August 2020
© Author(s) 2020. CC BY 4.0 License.

increasing nor decreasing over time). The deposition rate of sponge bSi has been estimated at 49.95 (± 74.14) mmol-Si m^{-2} yr^{-1} on continental margins, at 0.44 (± 0.37) mmol-Si m^{-2} yr^{-1} in sediment of ocean basins where sponge aggregations do not occur and at 127.30 (± 105.69) in deep-water sponge aggregations (Maldonado et al., 2019). By considering that the sponge aggregations occupy not more than 2% of seafloor at ocean basin, a corrected sponge bSi deposition rate for ocean basins is estimated at 2.98 (± 1.86) mmol Si m^{-2} yr^{-1} (Maldonado et al., 2019). When the average sponge bSi deposition rate for continental margins and seamounts (representing 108.02 Mkm^2 of seafloor) and for ocean basins (253.86 Mkm^2) is scaled up through the extension of those bottom compartments, a total value of 6.15 (± 5.86) Tmol-Si yr^{-1} can be estimated for the global ocean. If the production bSi that is being accumulated as standing stock in the living sponge populations annually is assumed to become constant in a long term equilibrium state, the global annual deposition rate of sponge bSi can be considered as a reliable estimate of the minimum value that the annual bSi production by the sponges can reach in the global ocean. The large associated SD value do not derive from the approach being little reliable but from heterogeneous spatial distribution on the marine bottom, with some ocean areas being very rich in sponges and sponge bSi in sediments while others are not.

5. Discussion

5.1 Overall residence times

The overall geological residence time for Si in the ocean (τ_G) is equal to the total amount of dSi in the ocean divided by the net input (or output) flux. We re-estimate the total ocean dSi inventory value derived from the Pandora model (Peng et al. 1993), which according to Tréguer et al. (1995) was 97,000 Tmol-Si. An updated estimate of the global marine dSi inventory was computed by interpolating the objectively analyzed annual mean silicate concentrations from the 2018 World Ocean Atlas (Garcia et al., 2018) to the OCIM model grid (Roshan et al., 2018). Our estimate is now 120,000 Tmol-Si, i.e. about 24 % higher than Tréguer et al. (1995)'s estimate. Taking this updated estimate of the total dSi inventory into account, Tables 1B and 3 show updated estimates of τ_G of Tréguer et al. (1995) and of Tréguer & De La Rocha (2013). Our updated budget (Fig. 1, Table 1B, Table 3A) reduces past estimates of τ_G (Tréguer et al., 1995; Tréguer and De La Rocha, 2013) by more than half, from ca.18 kyr to ca. 8 kyr (Table 3C). This brings the ocean residence time of Si closer to that of nitrogen (< 3 kyr, Sarmiento & Gruber, 2006) than phosphorus (30 – 50 kyr, Sarmiento & Gruber, 2006).

The overall biological residence time, τ_B, is calculated by dividing the total dSi content of the world ocean by gross silica production. Given the large uncertainty on our estimate of the bSi

https://doi.org/10.5194/bg-2020-274
Preprint. Discussion started: 3 August 2020
© Author(s) 2020. CC BY 4.0 License.

production by sponges it has been calculated from the bSi pelagic production only. τ_B is ca. 470 years (Table 1B, Table 3). Thus, Si delivered to the ocean passes through the biological uptake and dissolution cycle on average 17 times (τ_G / τ_B) before being removed to the sea floor (Table 1B, Table 3C).

The new estimate for the global average preservation efficiency of bSi buried in sediments is (7.0 /255=) 2.8 %, similar to Tréguer and De La Rocha (2013)'s estimate, and ~20 times larger than carbon preservation efficiency, making bSi in sediments a potential proxy for export production (Tréguer et al., 2018).

5.2 The issue of steady state

Over a given time scale, an elemental cycle is at steady state if the outputs balance the inputs in the ocean, and the mean concentration of the dissolved element remains constant.

5.2.1 Long time scales (>τ_G)

Over geologic time scales, the average dSi concentration of the ocean has undergone drastic changes. A seminal work (Siever, 1991) on the biological – geochemical interplay of the Si cycle showed a factor of 100 decline in ocean dSi concentration from 550 Myr to the present. This decline was marked by the rise of silicifiers like radiolarian and sponges during the Phanerozoic. Then, during the mid-Cenozoic, diatoms took control of a Si cycle previously dominated by inorganic and diagenetic processes. Taking into account the impact of the evolution of biosilicifying organisms (including bacterial-related metabolism), Conley et al., (2017) hypothesized that biological processes might also have influenced the dSi concentration of the ocean at the start of oxygenic photosynthesis. Demonstrated skeletal underdevelopment (Maldonado et al., 1999), and low performance in dSi consumption (Maldonado et al., 2020) in sponges when using dSi at the relatively modest concentrations typical of most environments in the modern ocean, also testify for sponges persisting maladapted to the important decrease in the average dSi concentration of the global ocean during the peak of molecular diversification and ecological expansion of diatoms over the Late Jurassic. Note that with a geological residence time of Si of about 8,000 years, the Si cycle can fluctuate over glacial-interglacial time scale.

5.2.2 Short time scales (< τ_G)

In the modern ocean, as shown above, the main control over silica burial and authigenic formation rate is the bSi production rate of (pelagic + benthic) silicifiers. The gross production of bSi due to diatoms is not Si-limited or not severely limited in several zones of the world ocean, which include the coastal zones, and the HNLC zones (Tréguer & De La Rocha, 2013). Thus, on short timescales, there are no strong negative feedbacks, between supply rates and

https://doi.org/10.5194/bg-2020-274
Preprint. Discussion started: 3 August 2020
© Author(s) 2020. CC BY 4.0 License.

production or burial rates, which would necessarily keep the marine Si cycle in balance. For this reason, climatic changes or anthropogenic impacts that affect dSi inputs to the ocean by rivers and/or other pathways, could lead to an imbalance of Si inputs and outputs in the modern ocean.

5.2.3 A possible steady-state scenario

Within the limits of uncertainty, the total net inputs of dSi and aSi are 14.8 (± 2.6) Tmol-Si yr^{-1}, and are approximately balanced by the total net output flux of Si with the conservative value of 13.4 (± 3.7) Tmol-Si yr^{-1}. Figure 1 shows a possible scenario for the Si cycle at steady state in the modern ocean, based on a balance of inputs and outputs at 14.8 Tmol-Si yr^{-1}, compatible with the geochemical and biological fluxes of Table 1. Raising the mean output flux up to 14.8 Tmol-Si yr^{-1} makes sense because of potential underestimation of different components of the present best-estimate total output flux. First, the value of F_B may be underestimated because the commonly used alkaline attack method (DeMaster, 1981) is not always effective at digesting all the bSi present in sediments, particularly bSi in highly silicified diatom frustules, radiolarian tests, or sponge spicules that are abundant in sediments (Maldonado et al., 2019). Second, our value of 4.7 Tmol-Si yr^{-1} value for F_{RW} is for the proximal coastal zone. However, reverse weathering reactions occur ubiquitously at the sediment water interface in the distal coastal zone, slope, and open ocean regions (Baronas et al., 2017; Ehlert et al., 2016a; Chong et al., 2016), suggesting that our present value for F_{RW} is an underestimate.

Consistent with Fig. 1, Figure 4 shows a possible steady-state scenario for the Si cycle in the coastal and continental margins zone (CCMZ), often called the "boundary exchange" zone which, according to Jeandel (2016) and Jeandel & Oelkers (2015), plays a major role in the land-to-ocean transfer of material (also see Fig. 2). Figure 4 illustrates the interconnection between geochemical and biological Si fluxes, particularly in the CCMZ. In agreement with Laruelle et al. (2009), Figure 4 also shows that the "open ocean" bSi production is mostly fueled by dSi inputs from below (94.3) Tmol-Si yr^{-1}) and not by the CCMZ (2.9 Tmol-Si yr^{-1}) (Supplement section 5).

5.3 Specific cases and unresolved questions

In the past three decades, best estimates for the net inputs or outputs of Si in and from the world ocean (Tréguer et a., 1995; Tréguer & De La Rocha, 2013) have increased by a factor of two. This is not only due to better spatial and temporal coverage of Si stocks and fluxes in the different regions of the world ocean, but also to a better understanding of the processes that control the Si cycle, such as SGD and reverse weathering (see discussion above). The two case

https://doi.org/10.5194/bg-2020-274
Preprint. Discussion started: 3 August 2020
© Author(s) 2020. CC BY 4.0 License.

studies herein presented illustrate the need to improve our understanding of the different contributions of dSi inputs in the coastal zone and the deep Pacific Ocean.

5.3.1 Chinese seas

In many respects, the Chinese marginal seas, composed of the Bohai Sea (BS), Yellow Sea (YS), East China Sea (ECS), and South China Sea (SCS), are a unique and interesting system to study the cycling of Si in the marine environment. Firstly, the dSi SGD inputs largely exceed the dSi riverine inputs by a factor of about 3-16 times for the BS, YS, and ECS (e.g. Ding et al., 2019; Liu et al., 2017a; Liu et al., 2017b; Wang et al., 2018b; Wu et al., 2017). Secondly, the bSi production seem to be mostly (62-90%) maintained by the recycling of Si (Li et al., 2019; Liu et al., 2005; Liu et al., 2016; Wu et al., 2017; Wu et al., 2020), which is unusual for coastal systems (Tréguer & De La Rocha, 2013). Thirdly, most (63-75%) of the bSi that reaches the sediment-water interface is accumulated in sediments (Li et al. 2019; Liu et al. 2005; Liu et al. 2016; Wu et al., 2017; Wu et al. 2020). Finally, reverse weathering as a sedimentary sink in the YS and in the SCS, could be a large component to the Si budget (Zhao et al., 2017). To date, preliminary Si budgets have been published for BS, YS and ECS (Li et al., 2019; Liu et al., 2005; Liu et al., 2016; Wu et al., 2017; Wu et al., 2020), but the estimates are still unbalanced since key fluxes, such as reverse weathering, are lacking. In addition, the relatively high load of lithogenic material in the Chinese marginal seas sediments, due to massive entrainment of siliceous soils through the hydrographic network of large rivers (Ding et al., 2019), make it difficult to quantify the bSi content in this system using a classic alkaline leach (DeMaster, 1981). We therefore recommend additional attention be paid to the cycling of Si within the Chinese marginal seas system in the near future.

5.3.2 The North-East Pacific dSi anomaly

Maximum dSi values Southern Ocean bottom waters are about 130 µM, but they are over 160-165 µM in the Pacific Ocean when the conveyor belt crosses the latitude of Hawaii. This dSi progressive enrichment is classically explained by recycling from siliceous debris in association with the biological pump. In the northern (> 50°N) Sea of Okhotsk, dSi concentrations exceed 200 µM at depths > 1,800 m, in a nitrate (> 40 µM) layer almost depleted in dissolved dioxygen. This Okhotsk system, acting as a natural sediment trap and biogeochemical processes, can fully account for this nutrient richness and O_2 depletion in bottom water. Exceptionally high dSi concentrations have been measured (e.g. P1 WOCE section at 47°N) on the eastern side of the North Pacific, where a large dSi rich plume contains concentrations > 200 µM-Si (Talley et al. 1992). The dSi total inventory of this plume is estimated at 164 Tmol-Si (Johnson et al., 2006), i.e. about 0.14 % of the world ocean inventory and it corresponds to an advective flux ranging

https://doi.org/10.5194/bg-2020-274
Preprint. Discussion started: 3 August 2020
© Author(s) 2020. CC BY 4.0 License.

between 1 and 2 Tmol-Si yr^{-1}. The process that feeds this dSi flux has not been identified yet, but possibilities include the dissolution of biogenic material accumulated on the deep valleys of this area, or hydrothermal fluids. Alternatively, this N-E Pacific dSi plume might be due to the remobilization of relatively old bSi that accumulated over a long time interval, a process that requires further studies as it would be considered as a net input for the Si cycle.

5.4 The impacts of global change on the Si cycle

As illustrated by Fig. 1 and 4, the pelagic bSi production is mostly fueled from the large, deep ocean recycled pool of dSi. This lengthens the response time of the Si cycle to changes in dSi inputs to the ocean due to global change (including climatic and anthropogenic effects), increasing the possibility for the Si cycle to be out of balance.

5.4.1 Impacts on riverine inputs of dSi and aSi

Climate change at short time scale during the 21st century impacts the ocean delivery of riverine inputs of dSi and aSi (F_R) and of the terrestrial component of the submarine groundwater discharge (F_{GW}), either directly (precipitations and subsequent dSi and aSi weathering and transport), or indirectly by affecting forestry and agricultural dSi export. So far, impacts of climate change and the terrestrial Si cycle have been reported for boreal wetlands (Struyf et al., 2010), North American rivers (Opalinka & Cowling, 2015), and for Arctic rivers which includes western Canadian Arctic (Phillips, 2020), and the tributaries of the Laptev and East Siberian Seas (Charette et al., 2020), but not for tropical environments. Tropical watersheds are the key areas for the transfer of terrestrial dSi to the ocean, as approximately 74% of the riverine Si input is from these regions (Tréguer et al., 1995). Note that, according to model predictions (Chou et al., 2004, 2008), under global warming, the precipitations in tropical regions usually follow “the rich-get-richer” mechanism. In other words, in tropical convergence zones rainfall increase with large climatological precipitations, but it is the reverse in tropical subsidence regions, with contradictory impacts for weathering of tropical soils. So, if the predicted global predictions of temperature rise and variations in precipitations of the IPCC are correct (IPCC, 2018), it is not sure that F_R or F_{GW}, two major components of dSi and aSi inputs, will increase at global scale by climate change during this century. Consistent with these considerations are the conclusions of Phillips (2020)’s first tentative to model the impacts of climate change on the riverine delivery of dSi to the ocean, using a machine learning. Using a model based on 30 environmental variables including temperature, precipitation, land cover, lithology, and terrain, Phillips (2020) predicts that within the end of this century, if dSi mean yield could increase regionally (for instance in the Arctic region), the global mean dSi yield is projected to decrease.

5.4.2 Abundance of marine and pelagic and benthic silicifiers

https://doi.org/10.5194/bg-2020-274
Preprint. Discussion started: 3 August 2020
© Author(s) 2020. CC BY 4.0 License.

Over the period 1960-2009, a change in diatom abundance was not seen on the North Atlantic from Continuous Plankton Recorder (CPR) data (Hinder et al., 2012). However, studies have cautioned that many fields (e.g. Chl) will take several decades before these changes can be significantly measured beyond natural variability (Henson et al 2010; Dutkiewicz et al 2019). Note that regarding the impact of climate change on benthic silicifiers, the melting of Antarctic ice platforms has been corroborated to trigger impressive population blooms of highly silicified sponges (Fillinger et al. 2013).

5.4.3. Predictions for the ocean phytoplankton production and bSi production

In the 21st century, climate change affects ocean circulation, stratification and upwelling thus affecting the cycles of nutrients (Aumont et al., 2003; Bopp et al., 2005, 2013). With increase stratification, reduced dSi supply from below (Fig. 1 and 4) leads to less siliceous phytoplankton production in surface compartments of lower latitudes and possibly the North Atlantic (Tréguer et al., 2018). The impact of climate change on the phytoplankton production or polar seas as is highly debated as melting of sea ice decreases light limitation. Regarding the Arctic Sea, increase nutrients (at the least for silicic acid) availability will occur through the Transpolar Drift delivering nutrient rich river- and shelf derived waters as potential sources for primary production, including bSi production (e.g. Charette et al., 2020). Regarding the Southern Ocean, bSi production is likely to increase in the coastal and continental shelf zone as iron availability increases due to ice – shelf and icebergs melting (Boyd et al., 1016; Hutchins & Boyd, 2016; Tréguer et al., 2018). Globally, it is therefore possible that a warmer and acidified ocean alters the pelagic bSi production rates, thus modifying the export production and outputs of Si at short time scales.

Although uncertainty is substantial, model studies (Bopp et al., 2005; Dutkiewicz et al., 2019; Laukötter et al, 2015) suggest regional shifting of bSi pelagic production due to climate change. Climate change models suggest a global decrease in diatom biomass and productivity over the course of the 21st century (Bopp et al., 2005, Dutkiewicz et al., 2019, Laufkötter et al., 2015), which would lead to a reduction in the pelagic biological flux of silica. Regional responses however differ, with most models suggesting a decrease in diatom productivity in the lower latitudes and many predicting an increase in diatom productivity in the Southern Ocean (Laufkötter et al, 2015). Holzer et al. (2019) suggest that changes in supply of dFe will alter bSi production mainly by inducing floristic shifts, not by relieving kinetic limitation. Increased primary productivity come from reduction in sea-ice and the faster growth rates with warmer waters and longer growing seasons in the high latitudes. However, many models have very simple ecosystems including only diatoms and a small phytoplankton. In these models,

https://doi.org/10.5194/bg-2020-274
Preprint. Discussion started: 3 August 2020
© Author(s) 2020. CC BY 4.0 License.

increased primary production in the Southern Ocean is mostly from diatoms. Some models with more complex ecosystem (i.e. including additional phytoplankton groups) suggest that increased primary productivity in the future Southern Ocean will be due to other phytoplankton types (e.g. pico-eukaryote) and that diatoms biomass will decrease (Dutkiewicz et al, 2019; also see model PlankTOM5.3 in Laufkötter et al, 2015), except in regions where sea-ice has melted. Differences in the complexity of the ecosystem and parameterizations, in particular in terms of temperature dependences of biological process, between models lead to widely varying predictions (Dutkiewicz et al., 2019; Laufkotter et al., 2015). These uncertainties suggest we should be cautious in our predictions of what will happen with the silica biogeochemical cycle in a future ocean.

5.4.2 Other anthropogenic impacts

For decades if not centuries, anthropogenic activities directly or indirectly altered the Si cycle in rivers, and the CCMZ (Bernard et al., 2010; Conley et al. 1993; Derry et al. 2005; Humborg et al., 2006; Ittekot et al., 2000, 2006; Laruelle et al. 2009; Liu et al., 2012; Yang et al., 2015; Wang et al., 2018; Zhang et al., 2019). Processes involved include eutrophication and pollution (Conley et al., 1993; Liu et al., 2012), river damming (Ittekot, 2006: Ittekot et al., 2000; Yang et al., 2015; Wang et al., 2018), deforestation (Conley, 2008), changes in weathering and in river discharge (Bernard et al. 2010; Yang et al. 2015), and deposition load in river deltas (Yang et al., 2015).

Among these processes, river damming is known for having the most spectacular and short time-scale impacts on the Si delivery to the ocean. In principle, river damming favours enhanced biologically mediated absorption of dSi in the dam reservoir, thus resulting in drastic decreases in dSi concentration downstream. Indeed, drastic perturbations on the Si-cycle and downstream ecosystem have been shown (Ittekot, 2006; Ittekot et al. 2000; Humborg et al. 2006; Zhang, 2019), particularly downstream of the Nile (Mediterranean Sea), the Danube (Black Sea) and the fluvial system of the Baltic Sea. This is critical for major rivers of the tropical zone (Amazon, Congo, Changjang, Huanghe, Ganges, Brahmaputra, etc.), which carry 74 % of the global exorheic dSi flux (Dürr et al., 2011; Tréguer et al., 1995). Among these major rivers, the course of Amazon and Congo are, so far, not affected by a dam or, if so for the Congo river, the consequence of Congo daming for the Si cycle in the equatorial african coastal system has not been studied. The case for Changjang (Yangtze), one of the major world players on dSi delivery to the ocean, is of particular interest. Interestingly, the Changjang (Yangtze) river dSi concentrations decreased dramatically from 1960s to 2000 (before the building of the Three Gorge Dam, TGD). As explained by Wang et al. (2018) this decrease is

https://doi.org/10.5194/bg-2020-274
Preprint. Discussion started: 3 August 2020
© Author(s) 2020. CC BY 4.0 License.

679 due a combination of natural and anthropogenic impacts. Paradoxically, since the achievement
680 of the TGD (2006 - 2009) no evidence of additional retention of dSi by the dam has been
681 demonstrated (Wang et al., 2018).
682
683 **6. Conclusions/recommendations**
684 The main question that still needs to be addressed is whether the contemporary marine Si cycle
685 is at steady state, which requires the uncertainty in total inputs and outputs to be minimized.
686 For the output fluxes, it is clear that the commonly used method for bSi determination
687 (DeMaster, 1981) in sediments does not fully account for the bSi contribution of siliceous
688 sponges and rhizarians, consequently the present value for silica burial is likely underestimated.
689 Quantitative determination of bSi is particularly difficult for lithogenic or silicate-rich
690 sediments (e.g. estuarine and coastal), for example those of the Chinese seas. An analytical
691 effort for the quantitative determination of bSi from a variety of sediment sources and the
692 organization of an international comparative analytical exercise are of high priority for future
693 research. It is also clear that reverse weathering processes are at work not only in estuarine or
694 coastal environments, but also in the distal coastal zone, slope, and open ocean regions of the
695 global ocean. Careful use of geochemical tools (e.g. ^{32}Si, Ge/Si, $\delta^{30}Si$) to trace partitioning of
696 bSi between opal and authigenic clay phases may further elucidate the magnitude of this sink,
697 particularly in understudied areas of the ocean.
698 For the input fluxes, more effort is required to quantify groundwater input fluxes, particularly
699 using geochemical techniques to identify the recycled marine flux from other processes that
700 generate a net input of dSi to the ocean. Studies addressing these uncertainties at the regional
701 scale are critically needed. Further, better constraints on hydrothermal inputs (for the North-
702 East Pacific specific case), aeolian inputs, and inputs from ice melt in polar regions are required.
703 Finally, in light of laboratory experiments by Fabre et al. (2019) demonstrating low temperature
704 dissolution of quartz in clastic sand beaches, collective multinational effort should address to
705 examine whether sandy beaches are major global dSi sources to the ocean.
706 This review highlights the significant progress that has been made in the past decade toward
707 improving our quantitative and qualitative understanding of the sources, sinks and internal
708 fluxes of the marine Si cycle. Filling the knowledge gaps identified in this review is also
709 essential if we are to anticipate changes in the Si cycle, and their ecological and biogeochemical
710 impacts, in the future ocean.
711
712

https://doi.org/10.5194/bg-2020-274
Preprint. Discussion started: 3 August 2020
© Author(s) 2020. CC BY 4.0 License.

Data avalaibility: All data used in this review article are available in the referenced articles. Data of biogenic pelagic production are shown in Supplement (Annex 1).

Supplement: The supplement related to this article is available on line at…XXX

Author contributions. PJT & JNS defined the manuscript content and wrote the paper. MAC, CE, JH, SR, OR & PT wrote the inputs section. JS, CE, SR, & MM wrote the outputs section. MB, TD, SD, AL, & PT wrote the pelagic production section. MLA & MM wrote the sponge subsections. SML, LR, & PT wrote the discussion section. Every author re-read and approved the review article.

Competing interests. The authors declare that they have no conflict of interest.

Acknowledgements. The idea for this manuscript was conceived during a conference of the SILICAMICS Network, held in June 2018 at the University of Victoria (Canada). This work was supported by the French National Research Agency (18-CEO1-0011-01). Thanks are due to Sébastien Hervé (LEMAR-IUEM, Plouzané) for his art work.

References

Aller, R. C., Blair, N.E., Xia, Q., & Rude, P.D.: Remineralization rates, recycling, and storage of carbon in Amazon shelf sediments, Cont. Shelf Res., 16, 753–786, 1996.

Aller, R.C.: Sedimentary diagenesis, depositional environments, and benthic fluxes, in: Treatise on Geochemistry: Second edition, edited by: Holland, H.D., & Turekian, K.K., Elsevier, Oxford, 8, 293–334, 2014.

Aller, R.C., Blair, N.E., & Brunskill, G.J.: Early diagenetic cycling, incineration, and burial of sedimentary organic carbon in the central Gulf of Papua (Papua New Guinea), J. Geophys. Res. Earth Surf., 113, 1-22, 2008.

Anschutz, P., Smith, T., Mouret, A., Deborde, J., Bujan, S., Poirier, D., Lecroart, P.: Tidal sands as biogeochemical reactors, Estuar. Coast. Shelf Sci., 84, 84–90, 2009.

Bevington, P.R., Robinson, D.K., 2003. Data Reduction and Error Analysis for the Physical Sciences, third ed., McGrawHill, NewYork, 2003.

Arsouze, T., Dutay, J. C., Lacan, F., & Jeandel, C.: Reconstructing the Nd oceanic cycle using

https://doi.org/10.5194/bg-2020-274
Preprint. Discussion started: 3 August 2020
© Author(s) 2020. CC BY 4.0 License.

745 a coupled dynamical - biogeochemical model. Biogeosciences, 6, 2829-2846, 2009.
746 Aumont, O., Ethé, C., Tagliabue, A., Bopp, L., & Gehlen, M.: PISCES-v2, an ocean
747 biogeochemical model for carbon and ecosystem studies, Geosci. Model Dev., 8, 2465–
748 2513, 2015.
749 Aumont, O., Maier-Reimer, E., Blain, S., & Monfray, P.: An ecosystem model of the global
750 ocean including Fe, Si, P co-limitations, Glob. Biogeochem. Cycles, 17, 1060,
751 doi:10.1029/2001GB001745, 2003.
752 Baines, S.B., Twining, B.S., Brzezinski, M.A., Krause, J.W., Vogt, S., Assael, D., McDaniel,
753 H.: Significant silicon accumulation by marine picocyanobacteria, Nat. Geosci., 5, 886–
754 891, 2012.
755 Baronas, J.J., Hammond, D.E., McManus, J., Wheat, C.G., & Siebert, C.A.: Global Ge isotope
756 budget, Geochim. Cosmochim. Acta, 203, 265-83, 2017.
757 Beck, A. J., Charette, M. A., Cochran, J. K., Gonneea, M. E., Peucker-Ehrenbrink, B.:
758 Dissolved strontium in the subterranean estuary - Implications for the marine strontium
759 isotope budget. Geochim. Cosmochim. Acta. 117, 33–52, 2013.
760 Behrenfeld, M. J., & Falkowski, P. G.: Photosynthetic rates derived from satellite-based
761 chlorophyll concentration, Limnol. Oceanogr., 42, 1-20, 1997.
762 Bernard, C.Y., Dürr, H.H., Heinze, C., Segschneider, J., & Maier-Reimer, E.: Contribution of
763 riverine nutrients to the silicon biogeochemistry of the global ocean – a model study,
764 Biogeosciences, 8, 551–564, 2011.
765 Bernard, C.Y., Laruelle, G.G., Slomp, C.P., & Heinze, C.: Impact of changes in river fluxes on
766 silica on the global marine silicon cycle: a model comparison, Biogeosciences, 7, 4441-
767 453, 2010.
768 Bopp, L., Resplandy, L., Orr, J.C., Doney, S.C., Dunne, J.P., Gehlen, M., Halloran, P., Heinze,
769 C., Ilyina, Séférian, R., Tjiputra, J., M. Vichi, M.: Multiple stressors of ocean
770 ecosystems in the 21st century: Projections with CMIP5 models, Biogeosciences, 10,
771 6225-6245, 2013.
772 Bopp, L., Aumont, O., Cadule, P., Alvain, S.,Gehlen, G.: Response of diatoms distribution to
773 global warming and potential implications: A global model study, Geophys. Res. Lett.,
774 32, L19606, 2005.
775 Boyd, P.W., Cornwall, C.E., Davison, A., Doney, S.C., Fourquez, M., Hurd, C.L., Lima, I.D.,
776 McMinn, A.: Biological responses to environmental heterogeneity under future ocean
777 conditions, Glob. Change Biol., 22, 2633-2650, 2016.

https://doi.org/10.5194/bg-2020-274
Preprint. Discussion started: 3 August 2020
© Author(s) 2020. CC BY 4.0 License.

778 Brzezinski, M.A., Krause, J.W., Baines, S.B., Collier, J.L., Ohnemus, D.C., Twining, B.S. :
779 Patterns and regulation of silicon accumulation in *Synechococcus* spp., J. Phycol. 53,
780 746–761, 2017.
781 Brzezinski, M.A., Baines, S.B., Balch, W.M., Beucher, C.P., Chai, F., Dugdale, R.C., Krause,
782 J.W., Landry, M.R., Marchi, A., Measures, C.I., Nelson, D.M., Parker, A.E., Poulton,
783 A.J., Selph, K.E., Strutton, P.G., Taylor, A.G., Twining, B.S.: Twining, Co-limitation
784 of diatoms by iron and silicic acid in the equatorial Pacific, Deep Sea Res. Part II Top.
785 Stud. Oceanogr., 58, 493–511, 2011.
786 Brzezinski, M.A.: The Si:C:N ratio of marine diatoms: Interspecific variability and the effect
787 of some environmental variables, J. Phycol., 21, 347–357, 1985.
788 Brzezinski, M.A. & Nelson, D.M.: Chronic substrate limitation of silicic acid uptake rates in
789 the western Sargasso Sea. Deep Sea Res. Part II Top. Stud. Oceanogr., 43, 437–453,
790 1996.
791 Brzezinski, M.A., & Phillips, D.R.: Evaluation of ^{32}Si as a tracer for measuring silica
792 production rates in marine waters, Limnol. Oceanogr., 42, 856–865, 1997.
793 Brzezinski, M.A., Villareal, T.A., & Lipschultz, F.: Silica production and the contribution of
794 diatoms to new and primary production in the central North Pacific, Mar. Ecol. Prog.
795 Ser., 167, 89–104, 1998.
796 Carr, M., Friedrichs, A.M., Schmeltz, M., Aita, M.N, Antoine, A., Arrigo, K.R., Asanuma, I,
797 Aumont, O, Barber, R., Behrenfeld, M., Bidigare, R., Buitenhuis, E.T., Campbell, J.,
798 Ciotti, A., Dierssen, H., Dowell, M., Dunne, J., Esaias, W, et al.: A comparison of global
799 estimates of marine primary production from ocean color, Deep Sea Res. Part II Top.
800 Stud. Oceanogr., 53, 741–770 (2006).
801 Charette M.A., Kipp, L.E., Jensen, L.T., Dabrowski, J.S., Whitmore, L.M., Fitzsimmons, J.N.,
802 Williford, T., Ulfsbo, A., Jones, E., Bundy, R. : The Transpolar Drift as a Source of
803 Riverine and Shelf-Derived Trace Elements to the Central Arctic Ocean, J. G. R.
804 Oceans, 125, [e2019JC015920], 2020, DOI:10.1029/2019jc015920
805 Chase, Z., Kohfeld, K.E., Matsumoto, K.: Controls on biogenic silica burial in the Southern
806 Ocean, Glob. Biogeochem. Cycles, 29, 1599–1616, 2015.
807 Cho, H.-M., Kim, G., Kwon, E.Y., Moosdorf, N., Garcia-Orellana, J., Santos, I.R.: Radium
808 tracing nutrient inputs through submarine groundwater discharge in the global ocean,
809 Sci. Rep., 8, 2439, 2018.
810 Chong, L.S., Berelson, W., Hammond, D.E., Fleisher, M.Q., Anderson, R.F., Rollins, N.E.,
811 Lund, S.: Biogenic sedimentation and geochemical properties of deep-sea sediments of

https://doi.org/10.5194/bg-2020-274
Preprint. Discussion started: 3 August 2020
© Author(s) 2020. CC BY 4.0 License.

812 the Demerara slope/abyssal Plain: Influence of the Amazon River Plume, Mar. Geol.,
813 379, 124-139, 2016.
814 Chou, C. & Neelin, J.D.: Mechanisms of global warming impacts on regional tropical
815 precipitations, J. Clim., 17, 2688-2701, 2004.
816 Chou, C., Neelin, J.D., Chen, C.-A., & Tu, J.-Y.: Evaluating the ‘‘rich-get-richer’’ mechanism
817 in tropical precipitation change under global warming, J. Clim., 22, 1982-2005, 2008.
818 Conley D.J, Likens, G.E., Buso, D.C., Saccone, L., Bailey, S.W., Johnson, C.E.: Deforestation
819 causes increased dissolved silicate losses in the Hubboard Brook Experimental Forest,
820 Glob. Change Biol., 14, 2458-2554, 2008.
821 Conley, D.J., Frings, P.J., Fontorbe, G., Clymans, W., Stadmark, J., Hendry, K.R., Marron,
822 A.O.,De La Rocha, C.L.: Biosilicification drives a decline of dissolved Si in the oceans
823 through geologic time, Front. Mar. Sci., 4, 397, 2017.
824 Conley, D.J., Schelske, C.L., & Stoermer, E.F.: Modification of the biogeochemical of silica
825 with eutrophication, Mar. Ecol. Progr. Ser., 101, 179-192, 1993.
826 De Souza, G.F., Slater, R.D., Dunne, J.P., & Sarmiento, J.L.: Deconvolving the controls on the
827 deep ocean’s silicon stable isotope distribution, Earth Planet. Sci. Lett., 398, 66–76,
828 2014.
829 DeMaster, D.J.: The accumulation and cycling of biogenic silica in the Southern Ocean:
830 revisiting the marine silica budget, Deep Sea Res. Part II Top. Stud. Oceanogr., 49,
831 3155–3167, 2002.
832 DeMaster, D.J.: The supply and accumulation of silica in the marine environment, Geochim.
833 Cosmochim. Acta, 45, 1715-1732, 1981.
834 Derry, L.A., Kurtz, A.C., Ziegler, K., & Chadwick, O.A.: Biological control of terrestrial silica
835 cycling and export fluxes to watershed, Nature, 433, 728-731, 2005.
836 Ding, S., Chen, P., Liu, S.M., Zhang, G., Zhang, J., Dan, S.F.: Nutrient dynamics in the
837 Changjiang and retention effect in the Three Gorges Reservoir. J. Hydrol., 574, 96–109,
838 2019.
839 Dunne, J.P., Sarmiento, J.L., & Gnanadesikan, A.: A synthesis of global particle export from
840 the surface ocean and cycling through the ocean interior and on the seafloor, Glob.
841 Biogeochem. Cycles, 21, GB4006 , 2007.
842 Dürr H.H., Meybeck, M., Hartmann, J, Laruelle, G.G., & Roubeix, V.: Global spatial
843 distribution of natural riverine silica inputs to the coastal zone, Biogeosciences, 8, 597–
844 620, 2011.
845 Dutkiewicz, S., Hickman, E., Jahn, O., Henson, S., Beaulieu, B. & Monier, E.: Ocean colour

https://doi.org/10.5194/bg-2020-274
Preprint. Discussion started: 3 August 2020
© Author(s) 2020. CC BY 4.0 License.

signature of climate change, Nat. Comm., 10, 019, 2019.

Dutkiewicz, S., Hickman, A.E., Jahn, O., Gregg, W.W., Mouw, C.B., & Follows, M.J.: Capturing optically important constituents and properties in a marine biogeochemical and ecosystem model, Biogeosciences, 12, 4447–4481, 2015.

Edmond, J.M., Measures, C., Mangum, B., Grant, B., F. R. Sclater, F. R., Collier, R.., Hudson, A., Gordon, L. I., Corliss, J. B.: On the formation of metal-rich deposits at ridge crests, Earth. Planet. Sci. Lett., 46, 19-30, 1976.

Ehlert, C., Doeringa, K. Wallmanna, K., Scholza, F., Sommera, S., Grasse, P., Geilerta, S., Frank, M.: Stable silicon isotope signatures of marine pore waters – Biogenic opal dissolution versus authigenic clay mineral formation, Geochim. Cosmochim. Acta, 191, 102–117, 2016a.

Ehlert, C., Reckhardt, A., Greskowiak, J., Liguori, B.T.P., Böning, P., Paffratha, R., Brumsack, H.-J., Pahnkea, K.: Transformation of silicon in a sandy beach ecosystem: insights from stable silicon isotopes from fresh and saline groundwaters, Chem. Geol., 440, 207–218, 2016b.

Elderfield, H. & Schultz, A.: Mid-ocean ridge hydrothermal fluxes and the chemical composition of the ocean, Ann. Rev. Earth Planet. Sci., 24, 191-224, 1996.

Escoube, R., Rouxel, O., Edwards, K., Glazer, B. and Donard, O.: Coupled Ge/Si and Ge isotope ratios as geochemical tracers of seafloor hydrothermal systems: case studies at Loihi Seamount and East Pacific Rise 9°50'N. Geochim. Cosmochim. Acta, 167, 93-112, 2015.

Fabre, S., Jeandel, C., Zambardi, T., Roustan, M., & Almar, R.: An overlooked silica source of the modern oceans: are sandy beaches the key? Front. Earth Sci., 7, 231, 2019.

Fillinger, L., Janussen, D., Lundälv, T., Richter, C.: Rapid glass sponge expansion after climate-induced Antarctic ice shelf collapse, Curr. Biol. 23, 1330-1334, 2013.

Franck, V.M., Brzezinski, M.A., Coale, K.H., & Nelson, D.M.: Iron and silicic acid concentrations regulate Si uptake north and south of the Polar Frontal Zone in the Pacific Sector of the Southern Ocean, Deep. Res. Part II Top. Stud. Oceanogr., 47, 3315–3338, 2000.

Frings, P.: Revisiting the dissolution of biogenic Si in marine sediments: a key term in the ocean Si budget, Acta Geochim, 36, 429–432, 2017.

Frings, P.J., Clymans, W., Fontorbe, G., De La Rocha, C.L., & Conley, D.J.: The continental Si cycle and its impact on the ocean Si isotope budget. Chem. Geol., 425, 12–36, 2016.

Galy, V.C., France-Lanord, C., Beysac, O., Faure, P., Kudrass, H., & Pahol, F.: Efficient

https://doi.org/10.5194/bg-2020-274
Preprint. Discussion started: 3 August 2020
© Author(s) 2020. CC BY 4.0 License.

organic carbon burial in the Bengal fan sustained by the Himalayan erosional system, Nature, 450, 407-410, 2007.

Garcia, H. E., Locarnini, R.A., Boyer, T.P., Antonov, J.I., Baranova, O.K., Zweng, M.M., Reagan, J.R., & Johnson, D.R.: Dissolved Inorganic Nutrients (phosphate, nitrate, silicate), in: World Ocean Atlas 2013, edited by Levitus, Mishonov A., NOAA Atlas NESDIS 76, 25 pp., 2014.

Geibert, W., Rutgers van der Loeff, M.M., Usbeck, R., Gersonde, R., Kuhn, G., Seeberg-Elverfeldt, J. : Quantifying the opal belt in the Atlantic and southeast Pacific sector of the Southern Ocean by means of ^{230}Th normalization, Glob. Biogeochem. Cycles, 19, GB4001, 2005.

Georg, R.B., West, A.J., Basu, A.R., & Halliday, A.N.: Silicon fluxes and isotope composition of direct groundwater discharge into the Bay of Bengal and the effect on the global ocean silicon isotope budget, Earth Plant. Sci. Lett., 203, 67-74, 2009.

Gnanadesikan, A., & Toggweiler, J.R.: Constraints placed by silicon cycling on vertical exchange in general circulation models. Geophys. Res. Lett., 26, 1865–1868, 1999.

Hatton, J.E., Hendry, K.R., Hawkings, J.R., Wadham, J.L., Kohler, T.J., Stibal, M., Beaton, A.D., Bagshaw, E.A., Telling, J.: Investigation of subglacial weathering under the Greenland Ice Sheet using silicon isotopes, Geochim. Cosmochim. Acta, 247, 191–206, 2019.

Hawkings, J. R., Hatton, J.E., Hendry, K. R., de Souza, G. F., Wadham, J. L., Ivanovic, R., Kohler, T. J., Stibal, M., Beaton, A., Lamarche-Gagnon, G., Tedstone, A., Hain, M. P., Bagshaw, E., Pike, J., Tranter, M.: The silicon cycle impacted by past ice sheets, Nat. Commun., 9, 3210, 2018.

Hawkings, J.R., Wadham, J.L., Benning, L.G., Hendry, K.R., Tranter, M., Tedstone, A., Nienow, P. & Raiswell, R. : Ice sheets as a missing source of silica to the polar oceans. Nat. Commun., 8, 14198, 2017.

Heinze, C., Hupe, A., Maier-Reimer, E., Dittert, N., & Ragueneau, O.: Sensitivity of the marine biospheric Si cycle for biogeochemical parameter variations, Glob. Biogeochem. Cycles, 17, 1086, 2003.

Henson, S. A., Sarmiento, J. L., Dunne, J. P., Bopp, L., Lima, I., Doney, S. C., John, J., Beaulieu, C.: Detection of anthropogenic climate change in satellite records of ocean chlorophyll and productivity, Biogeosciences, 7, 621–640, 2010.

Hinder, S. L., Hays, G. C., Edwards, M., Roberts, E. C., Walne, A. W., Gravenor, M. B.: Changes in marine dinoflagellate and diatom abundance under climate change, Nat.

https://doi.org/10.5194/bg-2020-274
Preprint. Discussion started: 3 August 2020
© Author(s) 2020. CC BY 4.0 License.

914 Clim. Chang., 2, 271–275, 2012.
915 Holzer, M., Primeau, F.W., DeVries, T., & Matear, R.: The Southern Ocean silicon trap: Data-
916 constrained estimates of regenerated silicic acid, trapping efficiencies, and global
917 transport paths, J. Geophys. Res. Ocean, 119, 313–33, 2014.
918 Hou Y., Hammond, D. E.; Berelson, W.M.; Kemnitz, N.; Adkins, J.F.; Lunstrum, A.: Spatial
919 patterns of benthic silica flux in the North Pacific reflect upper ocean production, Deep-
920 Sea Research Part I, 148, 25–33, 2019.
921 Humborg C., Pastuszak, M., Aigars, J., H. Siegmund, H., Mörth, C.-M., Ittekkot, V.: Decreased
922 silica land-sea fluxes trough damming in the Baltic Sea catchment –significance of
923 particle trapping and hydrological alteration, Biogeochemistry 77, 265-281, 2006.
924 Hutchins, D.A. & Boyd, P.W.: Marine phytoplankton and the changing ocean iron cycle. Nat.
925 Clim. Change, 6, 1072-1076, 2016.
926 Ittekkot, V, Humborg C, Schäfer P.: Hydrological alternations and marine biogeochemistry: a
927 silicate issue? BioScience, 50, 776–82, 2000.
928 Ittekot, V.,Unger, D., Humborg, C., Tac An, N. T. (Eds): The Silicon Cycle: Human
929 Perturbations and Impacts on Aquatic Systems, Comm. Probl. Environ. (SCOPE) Ser.
930 Vol. 66. Washington, DC: Island. 296 pp, 2006.
931 Jeandel, C.: Overview of the mechanisms that could explain the 'Boundary Exchange' at the
932 land–ocean contact, Philos. Trans. R. Soc. A Math. Phys. Eng. Sci., 374, 20150287,
933 2016.
934 Jeandel, C., Peucker-Ehrenbrink B., Jones, M.T., Pearce, C.R., Oelkers, E.H., Godderis, Y.,
935 Lacan, F., Aumont, O., Arsouze, T. : Ocean margins : the missing term for oceanic
936 element budgets ? Eos Trans. AGU, 92, 217, 2011.
937 Jeandel, C. & Oelkers, E.H.: The influence of terrigeneous particulate material dissolution on
938 ocean chemistry and global elements cycles, Chem. Geol., 395, 50-56, 2015.
939 Jin, X., Gruber, N. Dunne, J.P., Sarmiento, J.L., & Armstrong R.A.: Diagnosing the
940 contribution of phytoplankton functional groups to the production and export of
941 particulate organic carbon, $CaCO_3$, and opal from global nutrient and alkalinity
942 distributions, Glob. Biogeochem. Cycles, 20, GB2015, 2006.
943 Jochum, K. P., Schuessler, J.A., Wang, X.-H., Stoll, B., Weis, U., Müller, W.E.G., Haug, G.H.,
944 Andreae, M.O., Froelich, P.N.: Whole-ocean changes in silica and Ge/Si ratios during
945 the last deglacial deduced from long-lived giant glass sponges, Geophys. Res. Lett., 44,
946 555-564, 2017.

https://doi.org/10.5194/bg-2020-274
Preprint. Discussion started: 3 August 2020
© Author(s) 2020. CC BY 4.0 License.

947 Johnson, J.E., Goldfinger, C., Tréhu, A.M., Bangs, N.L.B., Torres, M.E., Chevallier, J., edited
948 by : Proceedings of the Ocean Drilling Program, 199 Scientific Results (Ocean Drilling
949 Program), 200).
950 Jones, M., Pearce, C.R., Oelkers, E.H.: An experimental study of the interaction of basaltic
951 riverine particulate material and seawater Geochim. Cosmochim. Acta, 77, 108-120,
952 2012.
953 Krause, J.W., Mark A. Brzezinski, M.A., Baines, S.B., Collier, J.L., Twining, B.S., Ohnemus,
954 D.C.: Picoplankton contribution to biogenic silica stocks and production rates in the
955 Sargasso Sea, Glob. Biogeochem. Cycles, 31, 762–774, 2017.
956 Krause, J.W., Brzezinski, M.A., Villareal, T.A., & Wilson, W.: Increased kinetic efficiency for
957 silicic acid uptake as a driver of summer diatom blooms in the North Pacific subtropical
958 gyre, Limnol. Oceanogr., 57, 1084–1098, 2012.
959 Laruelle, G.G., Roubeix, V., Sferratore, A., Brodherr, B., Ciuffa, D., Conley, D.J., Dürr, H.H.,
960 Garnier, J., Lancelot, Le Thi Phuong, Q., Meunier, J.-D., Meybeck, M.,
961 Michalopoulos, P., Moriceau, B., Ní Longphuirt, S., Loucaides, S., Papush, L., Presti,
962 M., Ragueneau, O., Regnier, P.A.G., Saccone, L., Slomp, C.P., , Spiteri, C., Van
963 Cappelle, P. : Anthopogenic perturbations of the silicon cycle at the global scale: key
964 role of the land-ocean transition, Glob. Biogeochem. Cycles, 23, GB4031, 1-17, 2009.
965 Laufkötter, C., Vogt, M., Gruber, Aita-Noguchi, M., Aumont, O., Bopp, L., Buitenhuis, E.,
966 Doney, S.C., Dunne, J., Hashioka, T., Hauck, J., Hirata, T., John, J., Le Quéré, C., Lima,
967 I.D., NakanoH., Seferian, R., Totterdell, I., Vichi, M., Völker, C.: Divers and
968 uncertainties of future global marine primary production in marine ecosystem models,
969 Biogeosciences, 12, 6955–6984, 2015.
970 Li, D., Dong, M., Liu, S., Chen, H., & Yao, Q.: Distribution and budget of biogenic silica in
971 the Yangtze Estuary and its adjacent sea, Sci. Total Environ, 669, 590–599 (2019).
972 Li, L, Barry, D.A., Stagnitti, F., & Parlange, J.Y.: Submarine groundwater discharge and
973 associated chemical input to a coastal sea, Water Resources Res., 35, 3253-3259, 1999.
974 Liu, J., Du, J., & Yi, L.: Ra tracer-based study of submarine groundwater discharge and
975 associated nutrient fluxes into the Bohai Sea, China: A highly human-affected marginal
976 sea, J. Geophys. Res. Ocean, 122, 8646–8660, 2017a.
977 Liu, J., Su, N., Wang, X., & Du, J.: Submarine groundwater discharge and associated nutrient
978 fluxes into the Southern Yellow Sea: A case study for semi-enclosed and oligotrophic
979 seas-implication for green tide bloom, J. Geophys. Res. Ocean, 122, 139–152, 2017b.
980 Liu, J., Zang, J., Bouwman, L., Liu, S., Yu, Z., Ran, X.: Distribution and budget of dissolved

https://doi.org/10.5194/bg-2020-274
Preprint. Discussion started: 3 August 2020
© Author(s) 2020. CC BY 4.0 License.

and biogenic silica in the Bohai Sea and Yellow Sea, Biogeochemistry, 130, 85–101 2016.

Liu, S.M., L.W., Zhang, G.L., Liu, Z., Yu, Z., & Ren, J.L.: Impacts of human activities on nutrient transports in the Huanghe (Yellow River) Estuary, J. Hydrol., 430-431, 103-110, 2012.

Liu, S.M., Zhang, J., & Li, R.X.: Ecological significance of biogenic silica in the East China Sea, Mar. Ecol. Prog. Ser., 290, 15–26, 2005.

Llopis Monferrer, N., Boltovskoy, D., Tréguer, P., Méndez Sandin, M., Not, F., Leynaert, A.: Estimating biogenic silica production of Rhizaria in the global ocean, Glob. Biogeochem. Cycles, 34, e2019GB006286, 2020.

Longhurst, A., S. Sathyendranath, T. Platt, Caverhill, C.: An estimate of global primary production in the ocean from satellite radiometer data, J. Plankton Res., 17, 1245–1271, 1995.

Longhurst, A.R. (Ed.) : Ecological Geography of the Sea, Academic Press, London, ed. 2nd, 2007.

Luijendijk, A., Hagenaars, G., Roshanka, R., Baart, F., Donchyts, G., Aarninkhof, S.: The state of the world's beaches, Sci. Rep., 8, 6641, 2018.

Maldonado M., Navarro L., Grasa A., Gonzalez A., Vaquerizo I.: Silicon uptake by sponges: a twist to understanding nutrient cycling on continental margins, Sci. Rep., 1, 30, 2011.

Maldonado, M., Ribes, M. & van Duyl, F. C. Nutrient fluxes through sponges, Adv. Mar. Biol., 62, 113–182, 2012.

Maldonado, M., López-Acosta, M., Beazley, L., Kenchington, E., Koutsouveli, V., Riesgo, A.: Cooperation between passive and active silicon transporters clarifies the ecophysiology and evolution of biosilicification in sponges. Sci. Advances, 6, 2020.

Maldonado, M., López-Acosta, M., Sitjà, C., García-Puig, M., Galobart, C.,Ercilla, G., Leynaert, A.: Sponge skeletons as an important sink of silicon in the global oceans, Nat. Geosci. 12, 815–822, 2019.

Matsumoto, K., Tokos, K., Huston, A., & Joy-Warren, H.: MESMO 2: a mechanistic marine silica cycle and coupling to a simple terrestrial scheme, Geosci. Model Dev. 6, 477–494, 2013.

Meire, L., Meire, P., Struyf, E., Krawczyk, D.W., Arendt, K.E., Yde, J.C., Pedersen, T.J., Hopwood, M.J., Rysgaard, S., Meysman, F.J.R.: High export of dissolve silica from the Greenland Ice Sheet, Geophys. Res. Lett. 43, 9173-9182, 2016.

Meyer, J. L., Jaekel, U., Tully, B. J., Glazer, B. T., Wheat, C. G., Lin, H.-T., Hsieh, C.-C.,

https://doi.org/10.5194/bg-2020-274
Preprint. Discussion started: 3 August 2020
© Author(s) 2020. CC BY 4.0 License.

1015 Cowen, J. P., Hulme, S. M., Girguis, P. R., Huber, J. A.: A distinct and active bacterial
1016 community in cold oxygenated fluids circulating beneath the western flank of the Mid-
1017 Atlantic ridge, Sci. Rep,. 6, 22541, 2016.
1018 Michalopoulos, P., & Aller, R. C.: Rapid Clay Mineral Formation in Amazon Delta Sediments:
1019 Reverse Weathering and Oceanic Elemental Cycles. Science, 270, 614–617, 1995.
1020 Michalopoulos, P. & Aller, R.C.: Early diagenesis of biogenic silica in the Amazon delta:
1021 alteration, authigenic clay formation, and storage, Geochim. Cosmochim. Acta, 68,
1022 1061-1085, 2004.
1023 Michaud, A. B., Skidmore, M. L., Mitchell, A. C., Vick-Majors, T. J., Barbante, C., Turetta,
1024 C., VanGelder, W., Priscu, J. C.: Solute sources and geochemical processes in
1025 Subglacial Lake Whillans, West Antarctica, Geology, 44, 347–350, 2016.
1026 Moriceau, B, Gehlen, M., Tréguer, P., Baines, S., Livage, J., André, L.: Editorial:
1027 Biogeochemistry and genomics of silicification and silicifiers, Front. Mar. Sci. 6, 57,
1028 2019.
1029 Morin, G.P., Vigier, N., & Verney-Carronc, A.: Enhanced dissolution of basaltic glass in
1030 brackish waters: Impact on biogeochemical cycles, Earth Planet. Sci. Lett., 417, 1–8,
1031 2015.
1032 Mottl, M.J.: Partitioning of energy and mass fluxes between mid-ocean ridge axes and flanks
1033 at high and low temperature, in: Energy and Mass Transfer in Marine Hydrothermal
1034 Systems, edited by Halbach, P.E., Tunnicliffe, V., Hein, J.R., Dahlem University Press,
1035 pp. 271–286, 2003.
1036 Nelson, D.M., & Goering, J.J.: Near-surface silica dissolution in the upwelling region off
1037 northwest Africa, Deep Sea Res., 24, 65–73, 1977.
1038 Nelson, D.M., Tréguer, P., Brzezinski, M.A., Leynaert, A., & Quéguiner, B.: Production and
1039 dissolution of biogenic silica in the ocean - Revised global estimates, comparison with
1040 regional data and relationship to biogenic sedimentation, Glob. Biogeochem. Cycles, 9,
1041 359–372, 1995.
1042 Ng, H.C., Cassarino, L., Pickering, R.A., Woodward, E.M.S., Hendry, K.R.: Sediment efflux
1043 of silicon on the Greenland margin and implications for the marine silicon cycle. Earth
1044 Planet Sci. Lett., 529, 115877, 2020.
1045 Nielsen, S. G., Rehkämper, M., Teagle, D. A. H., Butterfield, D. A., Alt, J. C. Halliday, A. N.:
1046 Hydrothermal fluid fluxes calculated from the isotopic mass balance of thallium in the
1047 ocean crust, Earth Planet. Sci. Lett., 251, 120–133, 2006.
1048 Ohnemus, D.C., Rauschenberg, S., Krause, J.W., Brezinski, M.A.: Silicon content of individual

https://doi.org/10.5194/bg-2020-274
Preprint. Discussion started: 3 August 2020
© Author(s) 2020. CC BY 4.0 License.

cells of *Synechococcus* from the North Atlantic Ocean, Mar. Chem., 187, 16–24, 2016.

Opalinka, B. & Cowlings, S.A.: Modelling the movement of biogenic silica from terrestrial vegetation to riverine systems within the continental USA, Ecol. Model., 312, 104-113, 2015. https://doi.org/10.1016/j.ecolmodel.2015.05.012

Pasquier, B., & Holzer, M.: Inverse-model estimates of the ocean's coupled phosphorus, silicon, and iron cycles, Biogeosciences, 14, 4125–4159, 2017.

Peng, T.-S. , Maier-Reimer, E., Broecker, W.S.: Distribution of ^{32}Si in the world ocean: model compared to observation. Glob. Biogeochem. Cycles, 7, 464-474, 1993.

Philipps, A. Modelling riverine dissolved silica on different spatial and temporalscales using statistical and machine learning methods, Ph.D thesis, Univ. Toronto, 121 pp., 2020. http://hdl.handle.net/1807/101210

Pichevin, L.E., Ganeshram, R.S., Geibert, W., Thunell, R., & Hinton, R.: Silica burial enhanced by iron limitation in oceanic upwelling margins, Nat. Geosci., 7, 2014.

Rahman, S., Aller, R.C., Cochran, & J.K.: Cosmogenic ^{32}Si as a tracer of biogenic silica burial and diagenesis: Major deltaic sinks in the silica cycle, Geophys. Res. Lett., 43, 7124–7132, 2016.

Rahman, S., Aller, R.C., & Cochran, J.K.: The missing silica sink: revisiting the marine sedimentary Si cycle using cosmogenic ^{32}Si, Glob. Biogeochem. Cycles, 31, 1559–1578, 2017.

Rahman, S., Tamborski, J.J., Charette, M.A., & Cochran, J.K.: Dissolved silica in the subterranean estuary and the impact of submarine groundwater discharge on the global marine silica budget, Mar. Chem., 208, 29–42, 2019.

Roshan, S., DeVries, T., Wu, J., & Chen, G.: The internal cycling of Zinc in the ocean, Glob. Biogeochem. Cycles, 32, 1833–1849, 2018.

Saconne, L., Conley, D.J., Koning, E., Sauer, D., Sommer, M., Kaczorek, D., Blecher, S.W., Kelly, E.F.: Assessing the extraction and quantification of amorphous silica in soils of forests and grassland ecosystems. Eur. J. Soil Sci., 58, 1446-1459, 2007.

Sarmiento, J.L. & Gruber, N. : Ocean biogeochemical dynamics, Princeton University press, Princeton & Oxford, 2006.

Sarmiento, J.L., Simeon, J., Gnanadesikan, A., Gruber, N., Key, R.M., Schlitzer, R.: Deep ocean biogeochemistry of silicic acid and nitrate. Glob. Biogeochem. Cycles, 21, GB1S90, 2007.

Siever, R.: Silica in the oceans: biological – geochemical interplay, in "Scientists in Gaia", edited by : Schneider, S.H. Boston, P.J., MIT Press, 285-295, 1991.

https://doi.org/10.5194/bg-2020-274
Preprint. Discussion started: 3 August 2020
© Author(s) 2020. CC BY 4.0 License.

1083 Struyf, E., Mörth, C.-M., Humborg, C., Conley, D.J.: An enormous amorphous silica stock in
1084 boreal wetlands, J.G.R., 115, G04008, 2010. doi:10.1029/2010JG001324.
1085 Syvistkia, J.P.M., Peckhama, S.D., Hilbermana, R., Mulderb, T.: Predicting the terrestrial flux
1086 of sediment to the global ocean:a planetary perspective, Sedim. Geol., 162, 5–24, 2003.
1087 Talley, L.D., Joyce, T.M.: The double silica maximum in the North Pacific. J. Geophys. Res.,
1088 97, 5465-5480, 1992.
1089 Techer, I., Advocat, T., Lancelot, J., & Liotard, J.M.: Dissolution kinetics of basaltic glasses:
1090 Control by solution chemistry and protective effect of the alteration film, Chem. Geol.,
1091 176, 235–263, 2001.
1092 Tegen, I. & Kohfeld, K.E.: Atmospheric Transport of Silicon, in: The silica cycle, human
1093 perturbations and impacts on aquatic systems, edited by Ittekot V. et al. anthropic, Scope
1094 66, 2006.
1095 Tréguer P. & Jacques, G.: Dynamics of nutrients and phytoplankton, and fluxes of carbon,
1096 nitrogen and silica in the Antarctic ocean, Pol. Biol., 12, 149-162, 1992.
1097 Tréguer, P., Louis Lindner, L., van Bennekom, A.J., Leynaert, A., Panouse, M., Jacques, G.:
1098 Production of biogenic silica in the Weddell-Scotia Seas measured with ^{32}Si, Limnol.
1099 Oceanogr., 36, 1217-1227, 1991.
1100 Tréguer, P., Nelson, D.M., Van Bennekom, A.J., Demaster, D.J., Leynaert,A., Quéguiner, B.:
1101 The balance of silica in the world ocean, Science, 268, 376-79,1995.
1102 Tréguer, P., Bowler, C., Moriceau, B., Dutkiewicz, S., Gehlen, M., Aumont, O., Bittner, L.,
1103 Dugdale, R., Finkel, Z., Iudicone, D., Jahn, O., Guidi, L., Lasbleiz, M., Leblanc, K.,
1104 Levy, M., Pondaven, P.: Influence of diatom diversity on the ocean biological carbon
1105 pump, Nat. Geosci., 11, 27–37 (2018).
1106 Tréguer, P., Pondaven P.: Silica control of carbon dioxide, Nature, 406, 358–359, 2000.
1107 Tréguer, P.J. & De La Rocha, C.L.: The World Ocean silica sycle, Ann. Rev. Mar. Sci., 5, 477–
1108 501, 2013.
1109 Tréguer, P.J.: The Southern Ocean silica cycle, Comptes Rendus Geosci., 346, 279–286, 2014.
1110 Usbeck, U.: Modeling of marine biogeochemical cycles with an emphasis on vertical particle
1111 fluxes, PhD thesis, University Bremen, 1999.
1112 Von Damm, K.L., Bischoff, J.L. and Rosenbauer, R.J.: Quartz solubility in hydrothermal
1113 seawater: An experimental study and equation describing quartz solubility for up to 0.5
1114 M NaCl solutions, Am. J. Sci., 291, 977-1007, 1991.
1115 Wang W., Yang, S., Ran, X., Liu, X.-M., Bataille, C.P., & Su, N.: Response of the Changjiang
1116 (Yangtze River) water chemistry to the impoundment of Three Gorges Dam during

https://doi.org/10.5194/bg-2020-274
Preprint. Discussion started: 3 August 2020
© Author(s) 2020. CC BY 4.0 License.

2010–2011, Chem. Geol. 487, 1–11, 2018.

Wang, X., Baskaran, M., Su, K., Du, J.: The important role of submarine groundwater discharge (SGD) to derive nutrient fluxes into river dominated ocean margins – The East China Sea, Mar. Chem., 204, 121–132, 2018.

Ward, B.A., Dutkiewicz, S., Jahn, O., & Follows, M.J.: A size-structured food-web model for the global ocean, Limnol. Oceanogr., 57, 1877–1891, 2012.

Westberry, T., Behrenfeld, M. J., Siegel, D. A., & Boss, E.: Carbon-based primary productivity modeling with vertically resolved photoacclimation. Glob. Biogeochem. Cycles, 22, GB2024 (2008).

Wheat, C.G., & McManus, J.: The potential role of ridge-flank hydrothermal systems on oceanic germanium and silicon balances, Geochim. Cosmochim. Acta, 69, 2021–2029, 2005.

Wheat, C.G., & Mottl, M.J.: Composition of pore and spring waters from Baby Bare: global implications of geochemical fluxes from a ridge flank hydrothermal system, Geochim. Cosmochim. Acta., 64, 629–642, 2000.

Wischmeyer, A.G., De La Rocha, C.L., Maier-Reimer, E., & Wolf-Gladrow, D.A.: Control mechanisms for the oceanic distribution of Si isotopes, Glob. Biogeochem. Cycles**,** 17, 1083, 2003.

Wu, B., Liu, S.M., & Ren, J.L. Dissolution kinetics of biogenic silica and tentative silicon balance in the Yellow Sea, Limnol. Oceanogr., 62, 1512–152, 2017.

Wu, B., Liu, S.M. Dissolution kinetics of biogenic silica and the recalculated silicon balance of the East China Sea. Science of The Total Environment https://doi.org/10.1016/j.scitotenv.2020.140552 (2020)

Yang S. L., Xu, K.H., Milliman, J.D., Yang, H.F., & Wu, C.S.: Decline of Yangtze River water and sediment discharge: Impact from natural and anthropogenic changes, Sci. Rep., 5, 12581, 2015).

Zhang, Z., Sun, X., Dai, M., Cao, Z., Fontorbe, G., Conley, D.J.: Impact of human disturbance on the biogeochemical silicon cycle in a coastal sea revealed by silicon isotopes, Limnol. Oceanogr., 65, 515-528, 2019.

Zhao, B., Yao, P., Bianchi, T., Xu, Y.: Early diagenesis and authigenic mineral formation in mobile muds of the Changjiang Estuary and adjacent shelf, J. Mar. Syst., 172, 64–74, 2017.

https://doi.org/10.5194/bg-2020-274
Preprint. Discussion started: 3 August 2020
© Author(s) 2020. CC BY 4.0 License.

Biogeosciences Discussions Open Access EGU

Table 1. Si inputs, outputs and biological fluxes at word ocean scale

A-Estimates for Si inputs and outputs		Reference	
Inputs (in Tmol-Si yr^{-1})			
$F_{R(dSi + aSi)}$ rivers	8.1 (±2.0)	Frings et al., (2016); Tréguer & De La Rocha (2013)	
F_A aeolian	0.5 (±0.5)	Tréguer & De La Rocha (2013)	
F_W dissolution lithogenic Si	1.9 (±0.7)	Tréguer & De La Rocha (2013)	
F_{GW} submar. groundwater	2.3 (±1.1)	Cho et al. (2018); Rahman et al. (2019); this review	
F_{ISMW} (sub)polar glaciers	0.3 (±0.3)	this review	
F_H hydrothermal	1.7 (±0.8)	this review	
Total inputs estimate	***14.8 (±2.6)***		
Outputs (in Tmol-Si yr^{-1})			
$F_{B(net\ deposit)}$ burial	7.0 (±2.3)	this review	
F_{SP} sponges	1 .7 (±1.6)	Maldonado et al. (2019)	
F_{RW} reverse weathering	4.7 (±2.3)	Rahman et al. (2016, 2017)	
Total outputs	***13.4 (±3.7)***		
B-Comparative estimates of Si fluxes			
	Ref. (1) & (2)	this review	Difference (%)
Net inputs (Tmol-Si yr^{-1})	9.4 (±4.7)	14.8 (±2.6)	+57 %
Net outputs (Tmol-Si yr^{-1})	11.4 (±7.6)	13.4 (±3.7)	+18 %
Gross bSi pelag. prod. (Tmol-Si yr^{-1})	240 (±40)	255 (±52)	+06 %
D : P (production: dissolution)	0.56	0.56	
τ_G residence time (kyears)	12.5(3)	8.1	-35 %
τ_B residence time (kyears)	0.50(3)	0.47	-6 %
$\tau_G : \tau_B$	25(3)	17	-32 %

Refs. (1) Nelson et al. (1995) (2) Tréguer & De La Rocha (2013).
(3) recalculated from our updated dSi inventory value
See Supplement for detailed definition of flux term (in detailed legend of Fig. 1).

https://doi.org/10.5194/bg-2020-274
Preprint. Discussion started: 3 August 2020
© Author(s) 2020. CC BY 4.0 License.

Table 2. Biological fluxes (F_{Pgross} in Tmol Si yr^{-1})
Global silica production as determined from numerical models and extrapolated from field measurements of silica production (uncertainties are standard errors)

	World Ocean	Coast	Southern Ocean	Open Ocean
Satellite Productivity models: - Chlorophyll level - Ocean Biogeochemical models	 207 (±23) 276 (±22)	56 (±18)	60 (±12) 129 (±19)	91 (±2)
Average of models	***242 (±49)***			
Silica production field studies: - Ocean basin[c] - Domain[c]	 249 285	 138	 67	 80
Average of field studies	***267 (±18)***			
Global estimate	**255 (±52)**			

https://doi.org/10.5194/bg-2020-274
Preprint. Discussion started: 3 August 2020
© Author(s) 2020. CC BY 4.0 License.

Biogeosciences Discussions

Table 3. Twenty-five years of evolution of the estimates for Si inputs, outputs, biological production, and residence times at world ocean scale

References : *(1)* Tréguer et al. (1995), *(2)* Tréguer & De La Rocha (2013), *(3)* this review, *(4)* Nelson et al. (1995)

A-Estimates for Si inputs and outputs fluxes

References	*(1)*	*(2)*	*(3)*
Inputs (Tmol-Si yr^{-1})			
$F_{R(dSi + aSi)}$ rivers	5.0 (±1.1)	7.3 (±2.0)	8.1 (±2.0)
F_A aeolian	0.5 (±0.5)	0.5 (±0.5)	0.5 (±0.5)
F_W dissolution lithogenic silica	0.4 (±0.3)	1.9 (±0.7)	1.9 (±0.7)
F_{GW} submar. groundwater	-	0.6 (±0.6)	2.3 (±1.1)
F_{ISMW} (sub)polar glaciers	-	-	0.3 (±0.3)
F_H hydrothermal	0.2 (±0.1)	0.6 (±0.4)	1.7 (±0.8)
Total inputs estimate	***6.1 (±2.0)***	***9.4 (±4.7)***	***14.8 (±2.6)***
Outputs (Tmol-Si yr^{-1})			
$F_{B(net\ deposit)}$ burial	7.1 (±1.8)	6.3 (±3.6)	7.0 (±2.3)
F_{SP} sponges	-	3.6 (±3.7)	1.7 (±1.6)
F_{RW} reverse weathering	-	1.5 (±0.5)	4.7 (±2.3)
Total outputs estimate	***7.1 (±1.8)***	***11.4 (±7.6)***	***13.4 (±3.7)***

B-Estimates for Gross production of biogenic silica (Tmol-Si yr^{-1})

References	*(4)*	*(3)*
Gross production of biogenic silica	240 (±40)	255 (±52)

C-Residence time of Si (kyears)

References	*(1)*	*(2)*	*(3)*
τ_G residence time (geological)	18.3(5)	12.5(5)	8.1
τ_B residence time (biological)	0.50(5)	0.50(5)	0.47
$\tau_G : \tau_B$	37(5)	25(5)	17

(5) recalculated from our updated dSi inventory value

https://doi.org/10.5194/bg-2020-274
Preprint. Discussion started: 3 August 2020
© Author(s) 2020. CC BY 4.0 License.

Figure 1: Schematic view of the Si cycle in the modern world ocean (input, output, and biological Si fluxes), and possible balance (total Si inputs = total Si outputs = 14.8 Tmol-Si yr^{-1}) in reasonable agreement with the individual range of each flux (F), see Tables 1 and 2. The white arrows represent fluxes of net sources of silicic acid (dSi) and/or of dissolvable amorphous silica (aSi) and of dSi recycled fluxes; Orange arrows correspond to sink fluxes of Si (either as biogenic silica and or as authigenic silica); Green arrows correspond to biological (pelagic) fluxes. All fluxes are in teramoles of silicon per year (Tmol-Si yr^{-1}). Details in Supplement section 1.

Figure 2. Schematic view of the low temperature processes that control the dissolution of (either amorphous or crystallized) siliceous minerals in seawater in and to the coastal zone and in the deep ocean, feeding F_{GW} and F_W. These processes correspond to both low and medium energy flux dissipated per volume of a given siliceous particle in the coastal zone, in the continental margins, and in the abysses, and to high-energy flux dissipated in the surf zone. Details in Supplement section 1.

Figure 3. Biogenic silica production measurements in the world ocean. Distribution of stations in the Longhurst biogeochemical provinces (Lonhurst, 2007; Longhurst et al., 1995). All data are shown in Supplement, section 4 (Annex 1).

Figure 4. Schematic view of the Si cycle in the coastal and continental margin zone (CCMZ), linked to the rest of the world ocean (« open ocean » zone, including upwelling and polar zones). In this steady-state scenario, consistent with Fig. 1, total inputs = total outputs = 14.8 Tmol-Si yr^{-1}. This figure illustrates the links between biological, burial and reverse weathering fluxes. It also shows that the "open ocean" bSi (pelagic) production ($F_{P(gross)}$ = 222 Tmol-Si yr^{-1}) is mostly fueled by dSi inputs from below (94.3 Tmol-Si yr^{-1}), the CCMZ only providing 2.9 Tmol-Si yr^{-1} to the "open ocean".

https://doi.org/10.5194/bg-2020-274
Preprint. Discussion started: 3 August 2020
© Author(s) 2020. CC BY 4.0 License.

1251 Figure 1

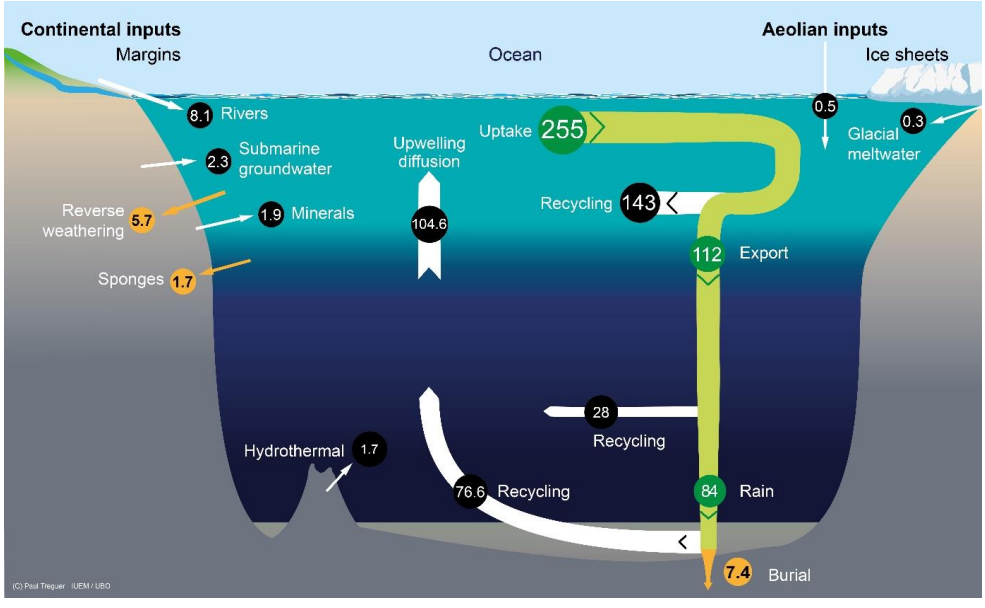

1252

1253

https://doi.org/10.5194/bg-2020-274
Preprint. Discussion started: 3 August 2020
© Author(s) 2020. CC BY 4.0 License.

Biogeosciences
Discussions
Open Access
EGU

1254 Figure 2

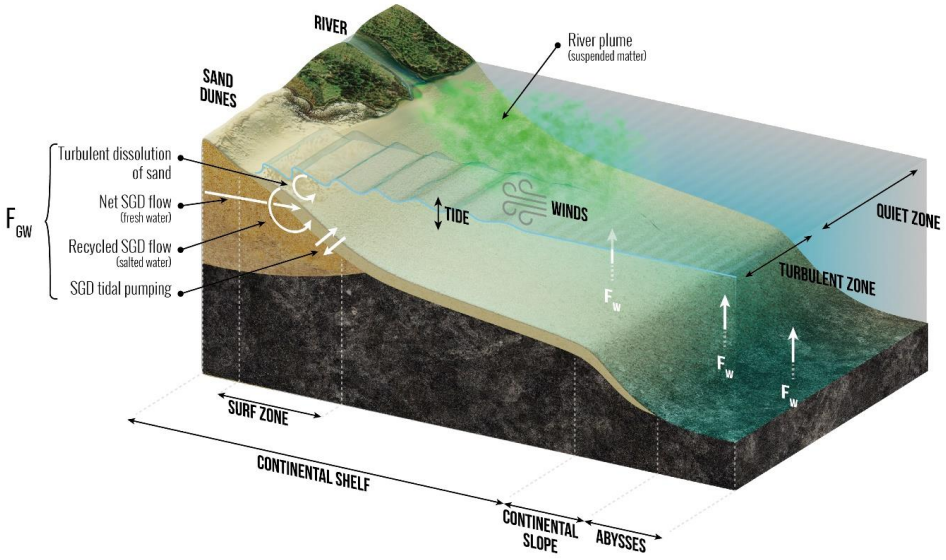

1255

1256

https://doi.org/10.5194/bg-2020-274
Preprint. Discussion started: 3 August 2020
© Author(s) 2020. CC BY 4.0 License.

1257 Figure 3

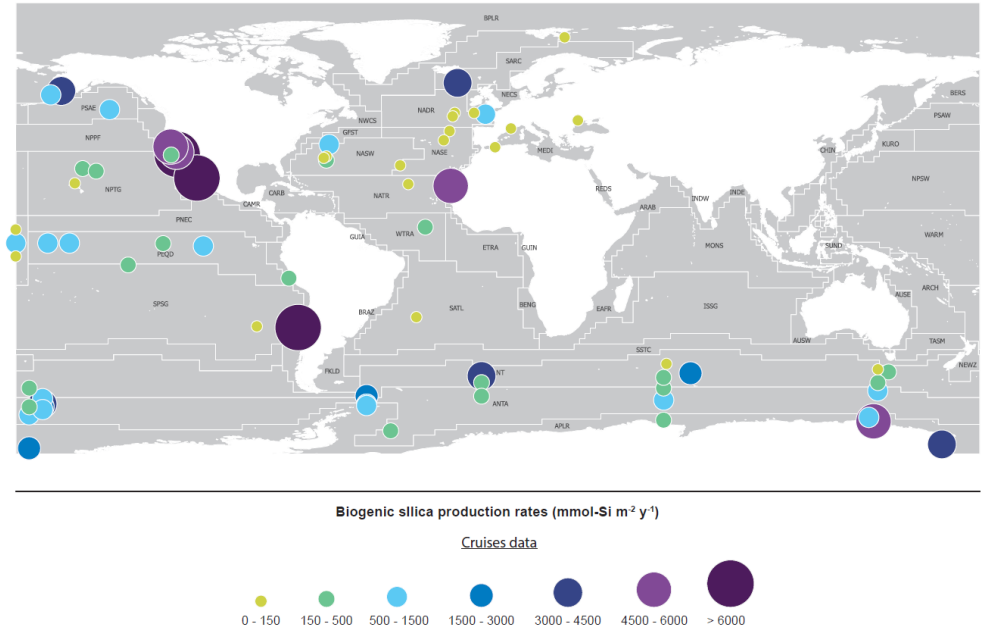

1258
1259

https://doi.org/10.5194/bg-2020-274
Preprint. Discussion started: 3 August 2020
© Author(s) 2020. CC BY 4.0 License.

1260 Figure 4

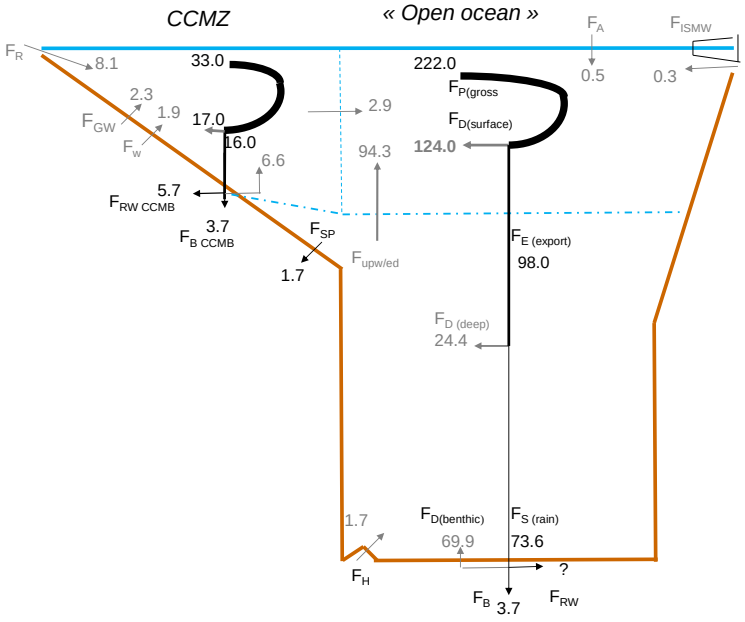

1261

1262